**SungEun Kim**

# A REVIEW ON RECENT DEVELOPMENTS IN FUSED DEPOSITION MODELING AND LARGE-SCALE DIRECT PELLET EXTRUSION OF POLYMER COMPOSITES

**Thesis**
**CENTRIA UNIVERSITY OF APPLIED SCIENCES**
**Environmental chemistry and technology**
**October 2020**

## ABSTRACT


| Centria University of Applied Sciences | Date | Author |
|---|---|---|
| | October 2020 | SungEun Kim |

**Degree programs**
Environmental Chemistry & Technology
Environmental, Process & Energy Engineering


**Name of the thesis**
A REVIEW ON RECENT DEVELOPMENTS IN FUSED DEPOSITION MODELING AND LARGE-SCALE DIRECT PELLET EXTRUSION OF POLYMER COMPOSITES


| Instructor | Pages |
|---|---|
| Rathish Rajan | 73 |

**Supervisor**
Jana Holm, Alexander Dumfort



Fused deposition modeling (FDM) and large-scale direct pellet extrusion has a potential on reducing material waste, energy consumption, and processing time compared to traditional manufacturing processes. However, these technologies deliver end parts with low mechanical properties resulting in failure when under load. In recent years, studies on improving the mechanical properties of printed parts has increased.

In this thesis, recent developments (2000-2020) in FDM and large-scale pellet extrusion of polymer composites are reviewed. To give a better understanding, FDM principle, feedstock materials, and main factors affecting the mechanical properties are described. Processing information such as input material, process equipment, process method, process temperature, nozzle diameter, and process parameters of each literature are tabulated and its influence on the end parts is described in the text. Tested process parameters such as type of reinforcing filler, filler infill, printing angle, printing width, printing layer height were also tabulated, and its effects were explained in the text.

Depending on the reinforced composite different effects on mechanical properties are shown. Increase of filler infill resulted in higher tensile properties and decrease of flexibility. However, after was reached of optimum value, this effect started to decrease. Structures produced in horizontal printing angle (0°), lower printing width, and lower printing height tend to show better mechanical properties. Large-scale production showed higher void formation, shrinkage, and residual stress than small-scale production leading to lower mechanical properties. These factors were reduced with extra process methods such as z-tamping, steel rod post-tensioning, pressure adjusting, compression wheel, MELT CORE printing head, in-box platform, water cooling system, vacuum robot, and nozzle with flexible head.

The concluded analysis of the reviewed literature only allows a general estimation. The collected literature had limitations to accurately compare the printed test specimens due to different process conditions and process parameters. The objective of future research would be to collect further literature with exact overlapping process conditions and process parameters for a better comparison.



**Key words**
Additive manufacturing, Fused deposition modeling, Large-scale direct pellet extrusion, Polymer composite, Mechanical properties

**ACKNOWLEDGEMENTS**

This thesis is part of ECOLABNET project funded by the European Union (European Regional Development Fund) under the Interreg Baltic Sea Region Programme 2014–2020.

Firstly, I want to share my appreciation to Rathish Rajan for directing and guiding me through the whole process of this thesis. He has shared his time to this project whenever possible and kept my motivation.

Secondly, I send my appreciation to my supervisors Jana Holm and Alexander Dumfort. Both have been one of the best professors in Centria University of Applied Science and Management Center Innsbruck who supported and motivated me throughout the whole double degree journey. I am thankful to have met and been taught by them.

Thirdly, I appreciate Nina Hynynen, as she dedicated her time to guide me during the studies and checked the language and layout of this thesis.

Lastly, my appreciation goes to my family, who has supported me during my whole studies. Also, I send out my thanks to all my friends, who made it possible for me to have an unforgettable study time in Kokkola, Innsbruck and Hammi village!

## ABBREVIATIONS AND CONCEPT DEFINITIONS

### Abbreviations

| | |
|---|---|
| ABS | Acrylonitrile butadiene styrene |
| AM | Additive manufacturing |
| AMIE | Additive Manufacturing Integrated Energy |
| CAD | Computer-aided design |
| CCFR | Continuous carbon fiber reinforcement |
| CF | Carbon fiber |
| C-FAB | Cellular fabrication |
| CM | Compression molding |
| DPE | Direct pellet extrusion |
| FDM | Fused deposition modeling |
| FFF | Fused filament fabrication |
| GF | Glass fiber |
| HDPE | High-density polyethylene |
| HDT | Heat deflection temperature |
| LDPE | Low-density polyethylene |
| LLDPE | Linear low-density polyethylene |
| MFI | Melt flow index |
| MIT | Massachusetts Institute of Technology |
| MWCNT | Multiwall carbon nanotube |
| ORNL | The Oak Ridge National Laboratory |
| PC | Polycarbonate |
| PE | Polyethylene |
| PEEK | Polyether ether keytone |
| PLA | Polylactic acid |
| POE-g-MA | Maleic anhydride polyolefin |
| PP | Polypropylene |
| PVA | Poly vinyl alcohol |
| RM | Rapid manufacturing |

| | |
|---|---|
| RP | Rapid prototypes |
| SL | Sheet lamination |
| SLA | Sterolithography |
| SLS | Selective laser sintering |
| STL | Stereolithography, Standard Triangulation Language |
| TPE | Thermoplastic elastomer |
| VGCF | Vapor grown carbon fiber |

**Concept definitions**

| | |
|---|---|
| Air gap | The distance of two near deposited filaments located in the same layer. It is also called print spacing. (Wu, Geng, Li, Zhao, Zhang &Zhao 2015.) |
| Ductility | It is a material measurement of the degree of plastic deformation that has been sustained at fracture (Rethwisch and Callister 2015). |
| Fill density | The fill density is in the range of 0 % to 100 %. It is the volume amount of material filled in the object. (Hodgson n.d.) |
| Flexural modulus | Flexural properties are measured to gain a measure of stiffness or rigidity. The flexural modulus in GPa is dependent on the testing temperature. The elastomer is quoted in MPa. (Bashford 1996.) |
| Flexural strength | This term is also known as modulus of rupture, fracture strength, or bend strength. It is the stress of material just before it yields in a flexural test. It is the highest stress within the material at its yield moment. (Rethwisch and Callister 2015.) |
| Glass transition temperature | The temperature where polymer experiences the transition from rubbery to a rigid state. The glass transition is shown in amorphous and semi-crystalline polymers due to the motion reduction of molecular |

| | |
|---|---|
| | chains with temperature decrease. It is referred to as $T_g$. (Rethwisch and Callister 2015, 488.) |
| Heat distortion temperature | This term is also known as the heat deflection temperature. It is defined as the temperature at which a specific distance deflection shows to a standard test bar under load. It indicates at what temperature the material starts to soften when exposed to load and elevated temperature. (ASTM D 648-18.) |
| Infill density | The volume percentage of one material compared by the whole filled volume of an object (Alani, Othman & Aliet 2018). |
| Near net shape | A post-process of the fabricated parts to meet wanted dimensional (ASTM 52900-15). |
| Porosity | Small voids in the system (ASTM 52900-15). It determines the void fraction of the total volume of the system (Kraxner 2002). |
| Printing angle 0° | The extrusion road is parallel to the long axis of the sample (Shofner, Lozano, Rodríguez-Macías, Barrera 2003). |
| Printing angle 45° | The extrusion road is 45° to the long axis of the sample (Shofner et al. 2003). |
| Printing angle 90° | The extruded road is perpendicular to the long axis of the sample (Shofner et al. 2003). |
| Strain | The deformation amount in the direction of the applied force is divided by the initial length of the material (Rethwisch and Callister 2015). |
| Stress | The loading of force is applied to the cross-sectional area of an object (Rethwisch and Callister 2015). |

| | |
|---|---|
| Tensile strength | It is a basic strength of a material. It is the maximum stress a material can withstand while stretched or pulled before breaking. Design stress which is used for design calculation is based on tensile strength. (Spruck 2019.) |
| Toughness | The material resistance to fracture when cracking (Rethwisch and Callister 2015). The ability of a material to deform elastically without fracturing. Balance of ductility and strength is required for high toughness. (Spruck 2019.) |
| X-axis | Axis in a machine coordinate system which runs in a parallel direction to the front of the machine and in a perpendicular direction to the y-axis and z-axis. The x-axis is commonly horizontal and parallel with one side edge of the build parts. When viewed from the front of the machine, the positive x-axis direction runs from left to right. (ASTM 52900-15.) |
| Y-axis | Axis in a machine coordinate system which runs in a perpendicular direction to the x-axis and z-axis. The y-axis is commonly horizontal and parallel with one side edge of the build parts. When viewed from the front of the machine, the positive y-axis direction runs from front to back of the machine and the negative y-axis direction runs from back to front. (ASTM 52900-15.) |
| Yield strength | It is quoted in MPa. The stress the material can resist without permanent deformation. (Bashford 1996.) |
| Young's modulus | This term is also known as the tensile modulus or modulus of elasticity. The material ability measurement to withstand changes in length while under lengthwise tension or compression. (Rethwisch and Callister 2015.) |

| | |
|---|---|
| Z-axis | Axis in a machine coordinate system which runs in a perpendicular direction to the y-axis and x-axis. When viewed from the front of the machine, the positive z-axis direction runs from the first deposited layer to the newest deposited layers. (ASTM 52900-15.) |

**TABLE OF CONTENTS**

**FIGURES**

**TABLES**

# 1 INTRODUCTION

Additive manufacturing (AM) is defined as the "process of joining materials to make parts from 3D model data, usually, layer upon layer" in the international standard ISO/ASTM 52900-15. (ASTM 52900-15.) It is also commonly known by the name "3D printing". (Keshavamurthy, Tambrallimath, and Saravanabavan 2021.) The term "add" in "additive" implements the technology which "adds up" volume elements, voxels, in a layer sequence. The produced physical model is based on a computer-aided design (CAD) virtual product file in a Stereolithography (STL) file form. (Pollack, Venkatesh, Neff, Healy, Hu, Fuenmayor, Lyons, Major & Devine 2019, 2; Gibson, Rosen & Stucker 2015, 352.) STL is a file format describing the object surface geometry as the tessellation of a triangle to communicate virtual shapes to AM machines. (ASTM 52900-15.) The 3D geometry model is divided into a series of finite 2D cross-section layers that vary in thickness. These CAD virtual data are translated by the AM machines and a physical form is built in one-layer on top of one-layer sequence. The material property of the fabricated product is generated during the building process by process factors such as the type of materials, process condition, production of layer, layer joining sequence and printing angle.

AM could be divided into seven process methods by the ISO/ASTM 52900-15 standard: binder jetting, direct energy deposition, material extrusion, material jetting, powder bed fusion, sheet lamination, and vat photopolymerization (ASTM 52900-15). Fused deposition modeling (FDM) technology which is a material extrusion type process, offers a simple fabrication process and a more cost-effective process compared to other AM technologies which bring high potential of FDM in the manufacturing field. (Gibson et al. 2015.) It is capable of manufacturing prototypes with complex geometries with reasonable dimensional accuracy. These advantages plus the expanded AM machine-processable filaments and pellets in the 2010s drew researchers' attention to develop FDM for application in industries such as health care, automotive, aerospace, and construction. Further, developments on direct pellet extrusion technology for large-scale parts have been rising. However, there are still disadvantages that have been identified, mainly related to the lower mechanical properties exhibited in FDM and large-scale direct pellet extrusion parts compared to the parts produced by conventional methods such as injection and compression techniques. For FDM and large-scale direct pellet extrusion technology to be used as an alternative method for conventional manufacturing processes, it needs to overcome the shortcoming of the method. This requires a solid understanding of FDM and large-scale direct pellet extrusion technologies based on current development. Therefore, the thesis aims to conduct a survey focused on recent developments and progress in the FDM technique and large-scale direct pellet extrusion

technology to understand the progress in these technologies and to list current challenges and the future direction. To achieve the aim, the thesis content is built as in Figure 1 with first introducing the principle of FDM, reviewing recent FDM researches on polymer composite, collecting developments on large-scale direct pellet extrusion, and concluding by discussing the questions in the figure.

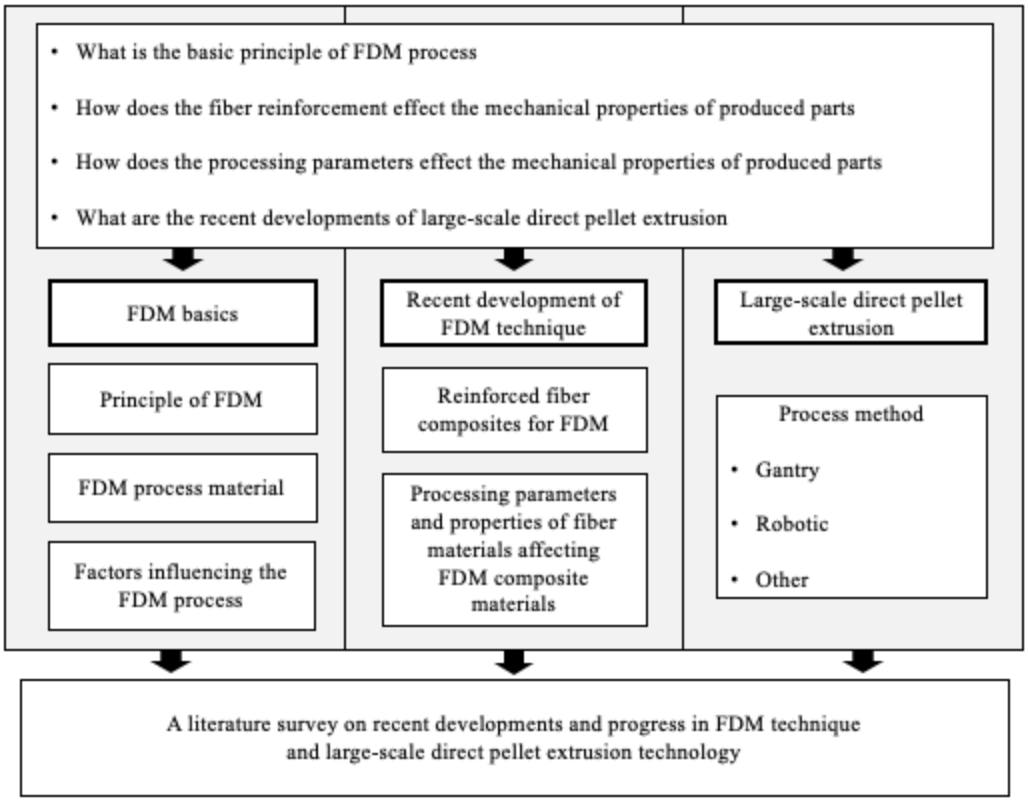


FIGURE 1. The content structure of this thesis

# 2 THEORETICAL BACKGROUND

In this chapter to give an overall view about AM technology, the development history of AM and the types of AM are explained. Further, theoretical background to understand the literature reviews are described by the process principle of FDM, the description of mechanical properties terms, the properties of frequently used FDM polymer matrix and types of polymer composite and finally the main factors affecting the mechanical properties of the produced parts.

## 2.1 General information about additive manufacturing

The AM technology can be divided into 2 categories depending on the level of its application: Rapid manufacturing (RM) and Rapid prototyping (RP), and into seven process methods by the ISO/ASTM 52900-15 standard. RM technology refers to the production of end parts and products. RP technology refers to the production of prototypes, mock-ups, and models emphasizing certain properties of the final product, allowing product capability tests for further production process development. RP was a historical term for AM technology in the late 1980s due to the limitation of the fabricated quality derived by a small studied range of usable material and process methods. (ASTM 52900-15; Gebhardt & Hötter 2016, 6-12.) The history of AM technology developments and description of the seven process types are explained in the sections below.

### 2.1.1 History of additive manufacturing

In the year 1956, one of the earliest concepts of AM, “Photo-glyph recording” described by Otto Munz was published. It functioned by creating solid layers at the air-liquid interface through the exposure of actinic radiation and continuous submerging of the fabricated objects into a vat of photoactive material. (Munz 1956.) In the year 1986, similar concepts of patents were filled in countries of Japan, France, and in the USA in terms of weeks. However, the patent from the USA filled by Charles Hull got generally recognized. This technology was the “Stereolithography” (SLA), noticed as the father of AM. Based on SLA technology Charles commercialized the first AM machine “Stereolithography apparatus-1” (SLA-1). (Hull 1986.) Further, in the same year of 1987, a file format of STL was introduced by the company where Charles was employed. This technology leads to communication between the AM machine and the CAD. In the next 10 years, other AM technologies such as “selective laser sintering” (SLS), “power

bed style printer", "sheet lamination" (SL), "fused deposition modeling" (FDM), "material jetting", "binder jetting" and "direct energy deposition" (DED) were introduced to the market. (Pollack et al. 2019,1-2.) The exact year of invention and developer of each technology can be seen in Table 1. In the 2000s the AM technology significantly improved with enhanced capability and widened processable materials of desktop printers of DLP, FDM, SLA, and SLS. This led to a significant cost drop, reaching the public in 2011. (Molitch-Hou 2018.)

TABLE 1. History timeline of AM technologies (adapted from Hull 1986; Molitch-Hou 2018; Munz 1956; Pollack et al. 2019,1-2.)

| **Year** | **Technology name** | **Developer** |
|---|---|---|
| 1956 | Photo glyph recording | Otto Munz |
| 1986 | Stereolithography | Charles Hull |
| | Stereolithography apparatus -1 stereolithography file format STL | Charles Hull from Ultraviolet |
| | Selective laser sintering | A patent from Carl Deckard and Joe Beaman. Cooperation of Helisys, Cubital, DTM |
| 1988 | Powder bed-style metal 3D print | A patent from Frank Arceclla |
| 1989 | 3D printing process | A patent from the Massachusetts Institute of Technology (MIT) group |
| 1991 | Sheet lamination | Company Helisys first introduced to the market |
| 1992 | Fused deposition modeling | Scott crump patent |
| | Selective laser sintering | Introduced in the market |
| 1993 | Material jetting | Commercialized and invented by Solid scape |
| | Binder jetting | MIT invented |
| | Inkjet | Sanders developed |
| 1996 | Binder jetting | Commercialized by Z corporation |
| 1997 | Direct energy deposition | Frank developed at Johns Hopkins University |
| 2011 | Desktop machines began to reach public appeal | |
| 2013 | Rise of low-cost Stereolithography and Digital light processing | |
| 2016 | Wide variety filaments could be printed on a desktop machine | |

### 2.1.2 Types of additive manufacturing

ISO/ASTM 52900-15 standard divided AM by seven process methods of binder jetting, direct energy deposition, material extrusion, material jetting, powder bed fusion, sheet lamination, and vat photopolymerization. (ASTM 52900-15.) Table 2 shows the ISO/ASTM 52900-15 standard definition of each process with subcategories of technology types, process principle, and its process materials

TABLE 2. Classification of additive manufacturing based on ISO/ASTM52900-15 (adapted from ASTM 52900-15; Camargo, Machado, Almeida & Silva 2019; Keshavamurthy et al. 2021; Pollack et al. 2019, 3-12; Molitch-Hou, 2018, 5-9).

| **AM methods** | **Process definition** | **Technology type** | **Process material** |
|---|---|---|---|
| Binder jetting | A liquid bonding agent is selectively deposited to join powder materials. | BJ<br>Binder jetting | metal, sand, ceramic, glass, calcium sulfate powder |
| Direct energy deposition | Focused thermal energy is used to fuse materials by melting as they are being deposited<br><br>"Focused thermal energy" means that an energy source (e.g., laser, electron beam, or plasma arc) is focused to melt the materials being deposited. | LENS<br>Laser engineering net shape<br>EBAM<br>Electron beam additive manufacturing | metals such as nickel-based alloys, aluminum |
| Material extrusion | Material is selectively dispensed through a nozzle or orifice | FDM/FFF<br>Fused deposition modeling/ Fused filament fabrication | polycarbonate (PC), acrylonitrile butadiene styrene (ABS), conductive acrylonitrile butadiene styrene, Polyphenylsulfone, PC-ABS blends, polyether ether ketone (PEEK), polyetherimide, wax, metals, ceramic, polylactic acid, high impact polystyrene resin |
| Material jetting | Droplets of build material are selectively deposited<br><br>Example materials include photopolymer and wax | MJ<br>Material jetting<br>NPJ<br>Nanoparticle jetting<br>DOD<br>Drop on demand | photopolymers, wax-like materials |

| | | | |
|---|---|---|---|
| Powder bed fusion | Thermal energy selectively fuses regions of a powder bed. | SLS<br>Selective laser sintering<br>MJF<br>Multi-jet fusion<br>SLM<br>Selective laser melting<br>EBM<br>Electron beam melting | polyamide (PA)<br>PA12, PA11, PA6<br>PEEK, nylon, thermoplastic elastomer, TPE, TPU<br>maraging steel, stainless steels, nickel-based superalloys |
| Sheet lamination | Sheets of material are bonded to form a part | LOM<br>Laminated object manufacturing | plastic sheet material, paper, polyvinyl chloride (PVC) |
| Vat photopolymerization | Liquid photopolymer in a vat is selectively cured by light-activated polymerization | SLA<br>Stereolithography<br>DLP<br>Digital light processing<br>CDLP<br>The continuous digital light processing | light photopolymerizing resin, Photocurable polymers, epoxy acrylate |

## 2.2 Principle of fused deposition modeling: A material extrusion technology

Fused deposition modeling is a material extrusion technology. It is also known in terms of fused filament fabrication (FFF). The basic principle of an extrusion technology is to add pressure force to a highly viscous material to extrude the material through a nozzle. Materials are forced out of the nozzle when pressure is applied to the reservoir of material. When the given pressure stays constant, the resulted cross-sectional diameter and the flow rate of the extruded material will remain constant. This diameter would remain the same when the movement of the nozzle will be kept at the same speed. The extruded material coming out of the nozzle must be in a semi-solid state and must solidify as regaining its shape. Also, the extruded material should bond to the layer below to result in a whole solid structure. The AM machine must be capable of moving the nozzle and the printing platform freely to build up the layer of the solid structure. To successfully extrude the material through the nozzle, the temperature is controlled to change the material state. (Gibson et al. 2015.)

The main characteristics of extrusion technology are (2.2.2) Loading of the material, (2.2.2) Liquification of material, (2.2.3) Extrusion, (2.2.4) Solidification, (2.2.5) Extrusion position control,

(2.2.6) Bonding, (2.2.7) Support generation and (2.2.8) Plotting. Each extrusion characteristic is separately described in the sections below.

### 2.2.1 Loading of the material

A continuous extrusion process is possible with a chamber. Chamber is where the preloaded materials are stocked. In an extrusion process, materials can be in a liquid or solid state which are in pellets, powders, or filaments form. In an FDM process, the materials are in a solid filament and pellet form. Materials in the chamber are fed continuously by gravity or by the support of a screw. The process that involves screw, generates pressure to the nozzle as well. (Gibson et al. 2015.)

### 2.2.2 Liquification of material

The loaded materials are mostly in pellets, powder, or filaments. These solid materials are not in a suitable form to be fed in the nozzle and they must be transformed. The transformation of the solid materials is done in the chamber with the addition of heat. The heat is normally applied by the heater coils wrapped around the chamber. The transformed material in the chamber should remain in a molten state but kept below its thermal decomposition temperature to prevent the production of residue inside the chamber. It is more a complex process to maintain the molten state of the material as the chamber gets larger. The parameters due to its heat transfer, thermal currents in the melt, location of temperature sensors, the physical state of the materials should be taken into mind. The liquified material gets pushed through the nozzle and will solidify followed by the extrusion process. (Gibson et al. 2015.)

### 2.2.3 Extrusion

The diameter of the extrusion nozzle affects the feature of the outflow and the size of the extruded filament. The nozzle diameter in FDM machines is manually changeable, however, throughout a specific build process, the diameter is usually constant. The nozzle diameter influences the shear rate, pressure drop, and printing width of the melt. The mass flow passing through the nozzle is managed by the pressure difference between the atmosphere surrounded and the chamber. (Gibson et al. 2015.) Higher pressure drops tend to show as the diameter decreases (Sukindar, Ariffin, Hang Tuah Baharudin, Jaafar

& Ismai 2016). Larger nozzle diameter can extrude more loading of material in a specific plotting speed, hence speeding up the build time however in a lower precision of the original CAD file. Besides, the nozzle diameter determines the minimum product size that can be created. The minimum product size is strictly followed so the feature produced could be provided with trustable strength. Therefore, extrusion-based products are more suitable for larger parts with features and wall thickness that are at least twice the nominal diameter of the extrusion nozzle. The thicker nozzle may be applied to build larger structures and smaller nozzles can be used for accurate structures. The nozzle shapes are circular, thus there are limitations on building sharp external and internal corners resulting rounding at corner areas. (Gibson et al. 2015.)

### 2.2.4 Extrusion positional control

Like other AM technologies, an extrusion-based system has a platform where products are formed. The extrusion head is located perpendicular (z-axis) to the platform to deposit material vertically to the platform. The extrusion head typically shows a horizontal (y-axis, x-axis) movement plotting. The extrusion plot setting is coordinated with the extrusion rate to establish a consistent deposition. Change in plotting direction result in a reduction in speed leading to non-consistent deposition. Therefore, the extrusion rate is lowered for a constant extrusion rate. (Gibson et al. 2015.)

### 2.2.5 Solidification

The material should ideally remain its shape once it is extruded. However, due to the effects of gravity and surface tension along with the effects of cooling and drying, the material deforms. The cooling and drying process is mostly nonlinear. The process of the molten material passing through a conical interface of the small nozzle adheres to materials. Deformations come in forms of shrinkage, warping or production of pores. Significant deformation brings changes to the desired quality of the final product. To reduce this phenomenon, the temperature difference between the chamber and the atmosphere could be kept minimum, and a controlled slow cooling process during the extrusion could be added. (Gibson, et al. 2015.)

The heat loss rate of the structure results in different ultimate deformation and internal stress. The temperature of the deposited parts will start to cool down as soon as the material is extruded. The cooling

rate depends on the geometry of the parts. Large and thick structures will maintain their heat longer than smaller and thinner structures due to the difference of surface to volume ratio. (Gibson, et al. 2015.) This deposited material loses its heat energy from the surrounding environment such as the atmosphere, the build platform, or the previously deposited layer (Compton, Post, Duty, Love & Kunc 2017).

### 2.2.6 Bonding

The feature can be built when extruded materials bond with the platform or the previous extruded layer. Heat based systems need sufficient residual heat energy on the material to activated the surface to the adjacent area as the residual heat energy causes bonding. The heat energy is supplied by the extrusion head. Therefore, the temperature of the extrusion head affects the bonding. In case of insufficient energy transfer, the parts would produce a boundary between the new and previous extruded material. This area could bring a fracture in the future. (Gibson, et al. 2015.)

### 2.2.7 Support generation

All AM technology needs a supporting system for keeping self-standing and disconnected feature parts in place during the fabrication process. FDM support can be divided into two general forms: Similar material supports and secondary material supports. Similar material support is for a simple method. As it only has one nozzle head, the material is the same. Adjustment of extrusion temperature can be made to purposely produce a fracture surface for separation to occur later. This boundary could be used for separating the supports and the final material parts. This process could be functioned by having additional distance when extruding the layer. The distance will affect the energy transfer rate and lead to fracture. A more sufficient way is secondary material supports. The fabrication of the supports would be indifferent materials. Secondary material support is structured with two extruders. One extruder is connected with the product material and the second extruder is connected with the support media material. The secondary material would be adjusted according to its parameter and would be extruded parallel with the build extruder. (Gibson, et al. 2015.)

### 2.2.8 Plotting

As all AM systems, extrusion machines receive the product information from CAD systems using an STL file format. (Gibson et al. 2015.) The STL file describes the object surface geometry by tessellation of the triangle. (ASTM 52900-15). The file format eases the extraction of the slice profile of the geometry and gives information on each slice. The software also determines the accuracy of fabrication, controlling the layer path, and extrusion head movements. As an example, the overfill extrusion points derived from the reduction of printing head speed at the start/stop and curve areas are calculated and the extrusion rate or the movement of the printing head is accelerated. This plotting outline determines the quality of the product. (Gibson, et al. 2015.)

The printing angle can greatly affect the mechanical properties of the produced parts. The most used printing angles are 45°, 0°, and 90°. The resulted dog bone shape samples plotted of different angles can be seen in Figure 2. (Tronvoll, Welo, and Elverum 2018.) The extrusion road is 45° to the long axis of the sample when printed at 45°, perpendicular at 90°, and parallel at 0° (Shofner et al. 2003). Depending on the material properties and the process conditions, the effect of the printing angle varies. (Tronvoll et al 2018.) Further influence of the printing angles on mechanical properties is explained in detail in experiment cases in chapters 3 and 4.

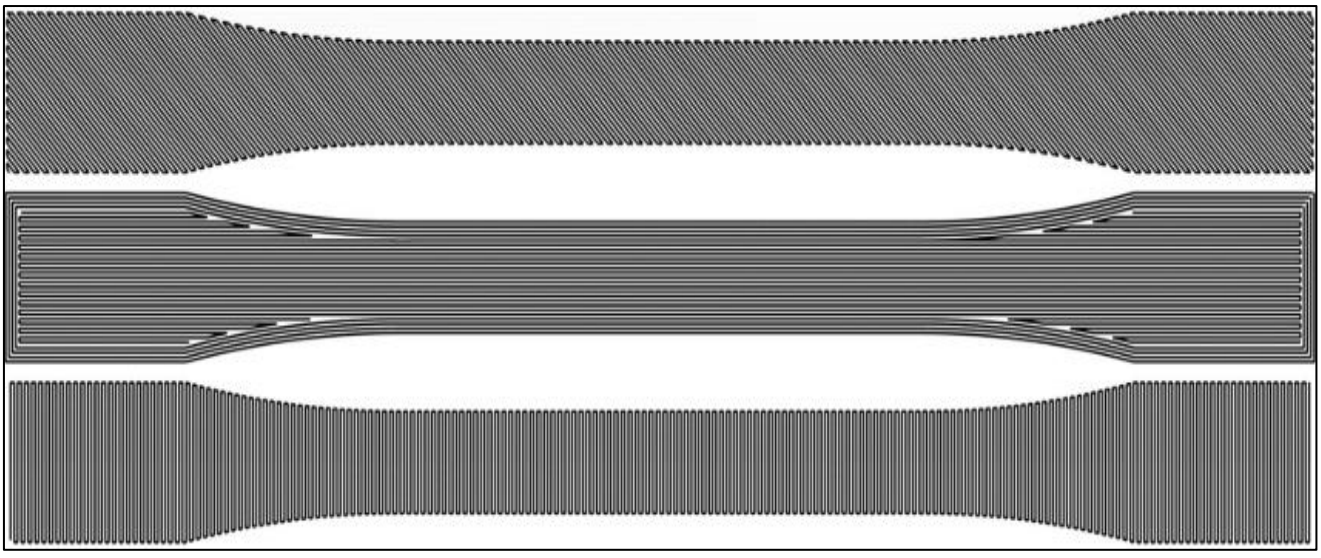

FIGURE 2. Printing angle of (a) 45°, (b) 0°, (c) 90° on dog bone shape sample (adapted from Tronvoll et al 2018.)

### 2.3 Understanding of mechanical properties: by a tensile stress-strain curve

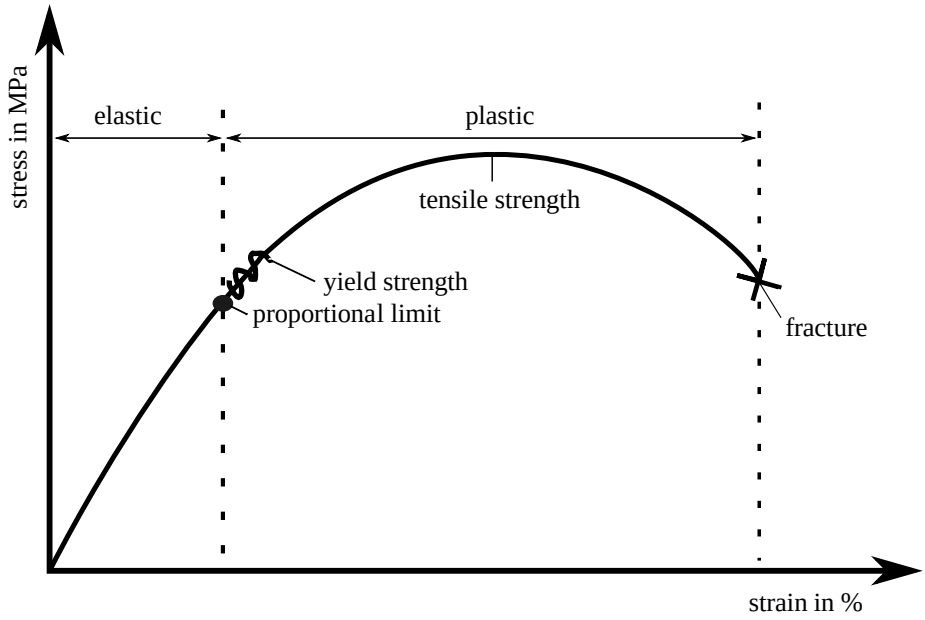


FIGURE 3. Tensile stress-strain diagram of a thermoplastic-like material (adapted from Stress-strain diagram, 2011.)

The stress-strain diagram plots the result from tensile tests. It graphically identifies important mechanical properties. The strain-stress diagram and its mechanical properties can be seen in Figure 3 for a better understanding of further explanation. The stress is a force per unit area that resulted from an applied load such as tension, shear, compression, torsion, or a combination of any. The strain is the material physical deformation in response to stress. It could also be explained as the elongation of the material. In the process of tensile testing, the force on the test specimen increases, and the strain proportionally increases. This is shown in a linear portion in the strain stress diagram which is called the elastic region. In a micro-level view of the test specimen, the bonds stretch in the elastic region and return to its original shape when the force is released resulting in no deformation. The slope of the elastic region defines the Young's modulus of the material, also known as the stiffness. As the applied load further increases, the test specimen will reach a point where the linear behavior is stopped. This point is the proportional limit. When little more loading is applied from this point, permanent deformation will take place. This point where deformation start is defined as yield stress. With additional force, the test specimen starts to neck, or diameter or thickness starts to decrease in size. This point is the tensile strength where maximum possible engineering stress is possibly applicable. Also, it is the highest point of the stress-strain curve at the stress y-axis. With more applied force from this point, the specimen will fracture with broken bonds. The region between the proportional limit point to the fracture point is called the plastic region.

It is important to not apply force beyond the yield strength or tensile strength at service to prevent failure from a mechanical engineering point of view. (Stress-strain diagram, 2011.)

## 2.4 Materials used in FDM printing process

In FDM, parts are produced by utilizing heat. Therefore, heat processable materials such as thermoplastics are generally used. However, the use of only polymer as FDM process material, results in fabricated parts with low mechanical properties. Therefore, fillers are added to the polymer to improve the material properties. This filler-reinforced polymer is called a composite. In the composites, the continuous phase of the reinforced material is the matrix. This functions as maintaining composite fillers in the proper orientation. (Gibson et al. 2015.)

### 2.4.1 Polymers

FDM operates better with polymer materials that are amorphous in nature than highly crystalline polymer. This is because the extrusion process is better in the viscous phase than in low viscosity form. Amorphous polymers do not have a definite melting point, instead as temperature increases, the material softens, and the viscosity decreases stepwise. The possible viscosity range of amorphous polymer is high enough to maintain the shape after extrusion and quickly solidify. Also, newly deposited material can easily bond with the previously deposited layer. The most common thermoplastics used in the FDM process are acrylonitrile butadiene styrene (ABS) and polylactic acid (PLA). Polyamide (PA), polyethylene (PE), polypropylene (PP), Teflon/polytetrafluoroethylene (PTFE), high impact polystyrene resin (HiPS), polyethylene terephthalate glycol (PETG), and polyether ether ketone (PEEK) are also used for FDM process. The glass transition temperature and printing temperature of FDM polymer materials which were collected in this thesis are listed in Table 3. (Gibson et al. 2015, 163-164.)

TABLE 3. Glass transition temperature and printing temperature of frequently used FDM polymer material. (adapted from Gibson et al. 2015, 163-164.)

| **Polymer material** | **ABS** | **PLA** | **LDPE** | **LLDPE** | **HDPE** | **PP** |
|---|---|---|---|---|---|---|
| Glass transition temperature in ℃ | 85-100 | 55-60 | -110 | -110 | -90 | -18 |
| Printing temperature in ℃ | 210-250 | 180-230 | 160-200 | 180-220 | 190-230 | 200-240 |

ABS is an amorphous copolymer consist of acrylonitrile, butadiene, and styrene (Walsh 2017). It has a glass transition temperature range of 85 to 100 ℃ (Domininghaus, Haim & Hyatt 1993, 190). Its softening point is approximately 100 ℃ and it begins to flow at around 200 ℃ (Zhong, Li, Zhang, Song & Li 2001). The printing bed temperature is in the range of 80 to 110 ℃ and its printing temperature is between 210 and 250 ℃, as ABS begins to decompose at around 250 ℃ (Walsh 2017). ABS has good mechanical properties, toughness, impact resistance, fluidity, and resistant to heat distortion (Rethwisch and Callister 2015). In addition, it has low water absorption and offers a lower risk of nozzle jamming compared to PLA (Bashford 1996). However, it exhibits large shrinkage resulting in low part accuracy. Hence, ABS is not biodegradable (Rethwisch and Callister 2015; Zhong et al. 2001). Approximately 90 percent of all FDM prototypes are produced with ABS. (Grimm 2002.) FDM experiments report that the ABS prototype has 60 to 80 percent strength of ABS injection molded parts, further with comparable thermal and chemical resistance. Every FDM machine offers ABS as a process material option (Shofner et al. 2003).

PLA is a synthetic biodegradable semi-crystalline polymer with a monomer of lactic acid derived from nature. (Jiang and Zhang 2017.) Its glass transition temperature is between 55 to 60 ℃ (Iannace, Sorrentino & Di Maio 2014). The printing temperature is between 180℃ and 230℃ with a printing bed temperature of 20 ℃ to 60 ℃ (Dey & Yodo, 2019 [PLA vs ABS Filament - Plastic strength, flexibility compared! Buyer's guide 2020]). PLA is a highly promising material due to its high rigidity, and ease of use (Sin, Rahmat & Rahman 2012). It has relatively higher tensile strength and lower warping and ductility compared to ABS. However, PLA is brittle which limits its use in high-performance requirements (Li, Li & Liu 2016).

PE is a semi-crystalline polymer and one of the most commonly used polymer in the world with a linear molecular structure of repeating $CH_2CH_2$- units. (Park and Seo 2011.) It has good thermal and basic properties that are easily processed at cheaper cost and has excellent resistance to acidic, basic, and

organic chemicals. The flexible property leads to easy processability. PE is suitable for water, marine, natural gas, and oil applications. (Walsh 2017.) PEs are differentiated by linearity, density, molecular weight, and molecular weight distribution and can be categorized. The often-used PE in the FDM process is the low-density polyethylene (LDPE), linear low-density polyethylene (LLDPE), and high-density polyethylene (HDPE). (Bashford 1996.)

LDPE has a structure containing short-chain branches (Rethwisch and Callister 2015, 128). LDPE has a glass transition temperature of -110 ℃, melting point range of 105 to 115 ℃, and process temperature range of 160 to 200 ℃. It has a good moisture resistance of less than 0.2 % absorption and excellent electrical insulation. However, is limited in durability with low thermal properties and mechanical properties with shrinkage of 2 to 5 %. (Bashford 1996.)

LLDPE has a glass transition temperature of -110 ℃ same with LDPE (Glass Transition Temperature (Tg) of Plastics - Definition & Values). LLDPE has a melting point range of 122 to 124 ℃ and a process temperature range of 180 to 220 ℃. It has a lower and higher range of serviceable temperatures than LDPE of the same density and melt index. It has a similar limitation as of LDPE with low engineering properties however with a better shrinkage range of 1.5 to 3 %. (Bashford 1996.)

HDPE has a primarily a linear structure (Rethwisch and Callister 2015, 128). HDPE has a glass transition temperature of -90 ℃, higher crystallinity than LDPE and LLDPE with a melting point range of 130 to 137 ℃, and process temperature of range 190 to 230 ℃. It has sufficient stiffness and strength for engineering uses. Also, it has good dynamic fatigue resistance and impact resistance with a wide temperature below to -40 ℃. However, HDPE has a high mold shrinkage and thermal expansion. (Bashford, 1996; Rethwisch & Callister, 2015, 490.)

PP is a semi-crystalline polymer that is categorized in a non-polar polyolefin (Sodeifian, Ghaseminejad & Yousefi 2019). It has a repeat unit similar to that of PE except that a methyl ($CH_3$) group replaces one of the hydrogen atoms. It has a specific gravity of 0.90 g/cm$^3$ being the lightest among the most common thermoplastic when unmodified. (Baker 2018; Walsh 2017.) Its glass transition temperature is -18 ℃, melting point is 165 ℃ , and processing temperatures are in the range of 200 to 240 ℃. (Bashford, 1996; Rethwisch & Callister, 2015, 490.) PP shows embrittlement under -17 ℃ and its heat deflection temperature is between 91 to 116 ℃ (Walsh 2017). PP has a good thermal resistance compared to PLA. (Sodeifian et al. 2019.) In addition, it has unique properties such as low density, non-toxicity, re-

processability, good electrical properties, high resistance to acids, base, oil, and hot water, and is available at a reasonable price. However, PP is not recommended with aromatic chemicals, oxidizing acids, or chlorinated hydrocarbons. (Sodeifian et al. 2019; Walsh 2017.) PP can be used for low-stress structural applications up to 135 ℃ and in water handling applications as it has low water absorption. Further, it is used in a wide range of applications such as the textile industry, food packaging, medical facilities, piping, construction, and automotive industries (Sodeifian et al. 2019).

### 2.4.2 Polymer composites

Composite is generally defined as a combination of two or more materials resulting in a new material with better properties than the individual components. Each material maintains its chemical, physical, and mechanical properties when combined. Fiber/filler material improves strength and stiffness to the matrix, hence most of the reinforced composite has better material properties. In Figure 4, tensile strength and strain property of fiber, composite, and matrix can be seen. (Campbell 2010.)

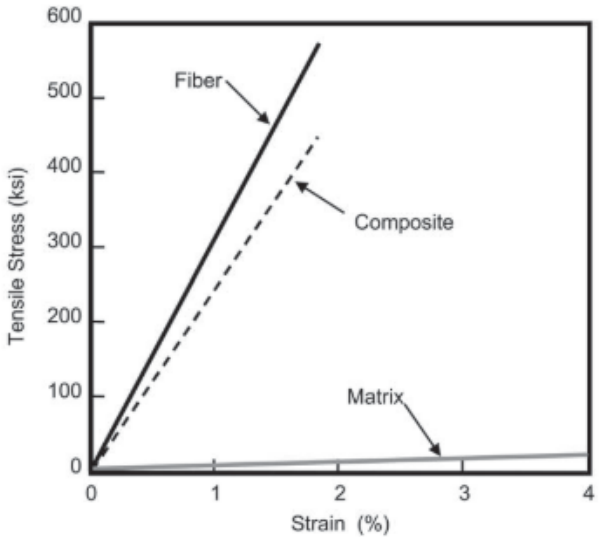


FIGURE 4. The general tensile stress and strain value of composite, fiber, and matrix (adapted from Campbell 2010.)

A limit of 70 volume percent of reinforcing fiber is derived by practical experiments. The practical cut-off is also applied in the data of Figure 4. A higher percentage of fiber results in insufficient adhesion between fibers and matrix due to little matrix. In FDM printing process composite materials must be in a filament form. (Campbell 2010; Wang, Jiang, Zhou, Gou & Hui 2017.)

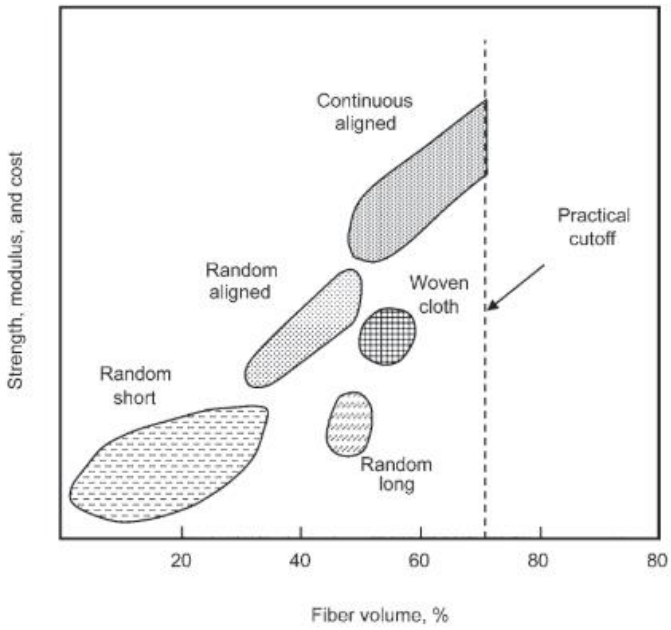


FIGURE 5. The composite performance on strength, modulus, and cost depending on the reinforcement type (adapted from Campbell 2010.)

Fiber has a greater length than its diameter. The length-to-diameter ratio is called the aspect ratio. This ratio differs with every reinforcing fiber depending on its dimensions. Depending on the length of the fiber, the reinforced fiber composites can be categorized into short fiber reinforced composites (discontinuous fiber composite), continuous fiber reinforce composite, nanocomposite, and particulate composite. (Heidari-Rarani, Rafiee-Afarani, and Zahedi 2019.)

Short fiber has a short aspect ratio. Examples of a short fiber composite can be polymers reinforced with chopped fibers and random mat (Krishnaprasad, Veena, Maria, Rajan, Skrifvars & Joseph 2009). Short fiber composites are usually randomly aligned in composite parts. This factor reduces strength and modulus. However, short fiber composite usually costs less than a continuous fiber composite. (Campbell 2010.)

Continuous fiber has a long aspect ratio having a preferred orientation. (Campbell 2010.) This leads to uniform fiber orientation resulting in equal material properties throughout the parts (Peltola 2019). In Figure 5, it is shown that the highest modulus and strength are achieved by continuous fiber composite. (Campbell 2010.) Examples of the continuous composite can be knitted (Matsuzaki, Ueda, Namiki, Jeong, Asahara, Horiguchi, Nakamura, Todoroki & Hirano 2016) or stitched unidirectional fabrics, woven fabric (Fantuzzi, Bacciocchi, Agnelli & Benedetti 2020), processed carbon fiber (Heidari-Rarani et al. 2019), and helical winding (Ke, Wu, Liu, Xiang & Hiu 2020). In FDM processes, continuous fiber

composites are usually laminated by polymer matrix in different orientations to achieve the necessary properties of strength and stiffness (Matsuzaki et al. 2016).

Nanocomposite is formed with at least one phase with a dimension of a nanometer range. The structural forms of the nano-sized filler are as particle, fiber, nanotube, and whiskers. Examples of nanocomposite fillers can be single or multi-walled carbon nanotube and vapor grown carbon fiber. Nanofiller aggregation and orientation in polymer matrix are an important structural phenomena which influence the properties of the structure. Nanofiller interfacial interaction is assumed to be larger than traditional composite due to assumption of a significantly large interfacial area. (Din, Shah, Sheikh & Mursaleen 2019; Hári and Pukánszky 2011.)

Particulate composite is contained with at least one phase starting with a discrete solid in size range smaller than 1 mm. The second phase could be in form of a molten polymer. Examples of particulate composite fillers are titanium dioxide ($TiO_2$), copper powder, iron powder, glass fiber, and graphite particles. Particulate composite results in isotropic characteristics. (German 2016, 2-8.)

## 2.5 Main factors affecting the mechanical properties of the polymer composites printed by fused depositing method

Morphological analysis provides structural defects of the produced parts. The useful information derived from the morphological analysis are the voids, micro-cracks, fusion quality between the matrix and fiber of the produced parts. These parameters impact the mechanical properties of the produced parts. (Heidari-Rarani et al. 2019.)

### 2.5.1 Voids

Two types of voids could be produced during the fabrication process: inner-bead voids and inter-bead voids. Inner-bead voids are caused by low adhesion force between reinforcing fiber and polymer matrix. The voids tend to increase when the presence of fiber increases. Voids inside the beads result in concentrated stress points causing low impact resistance, elongation to break, and fail at lower stresses. Inter-bead voids are derived during the cooling process of bead deposition. It tends to build up in a downward-triangular shape aligned by the printing direction. The triangular voids can be seen in Figure

6. This results in linear defects on properties. (Tekinalp et al. 2014; Wang, Xie, Weng, Senthil & Wu 2016.) Also, voids could be caused by the volatilization of low molecular weight material during heat-extrusion or from entrapped air in the pellet or filament feedstock (Duty, Kunc, Compton, Post, Erdman, Smith, Lind, Lloyd & Love 2017).

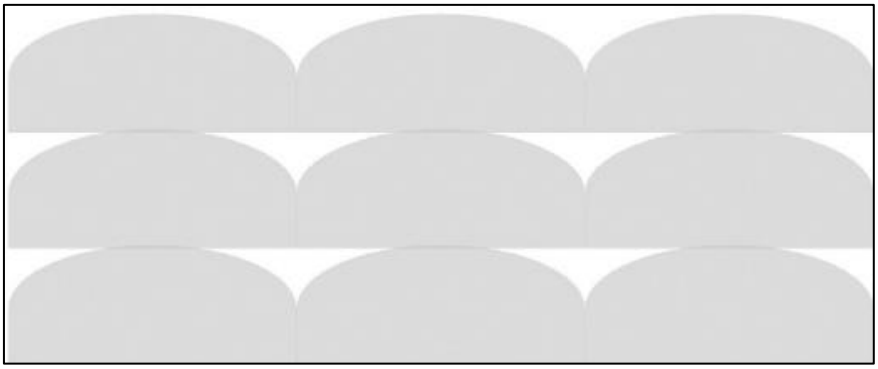

FIGURE 6. A cross-section of the FDM fabricated part showing the inter-bead voids (adapted from Wang et al. 2016.)

### 2.5.2 Fiber orientation

Uniformity in the properties to the built structure is derived with an even concentration of composites. Careful adjustment of extruder set-up and feeding is done to control distribution and dispersion. Uneven distribution as agglomeration results in internal stress to the material. Isotropic fibers are least deleterious to elongation to break however causes a slight decrease to yield strength. In addition, the distribution direction of fibers such as unidirectional, oriented, or random oriented results in different mechanical properties. (DeArmitt 2017.) Dispersants can be used to result good dispersion when using fine or nanoparticles (Gupta and Bijwe 2020). The shear force produced in extruders decreases the dispersion and of particles. Further influence of fiber orientation is explained in detail in experiment cases of chapters 3 and 4.

### 2.5.3 Fiber length

Short fiber length results in high viscosity leading to low processability and difficulty in extrusion. It is difficult to evenly disperse small particles as it tends to agglomerate. In reality, nanoparticles are not used often due to its high agglomeration and its expensive production cost which in the end is cost-inefficient. Large fiber length results in high-stress concentration around the large particles. This leads to dramatic reduction in impact resistance and elongation break value. (DeArmitt 2017, 517-532.) In Figure 7 the distribution of particles and its effect on material properties are shown.

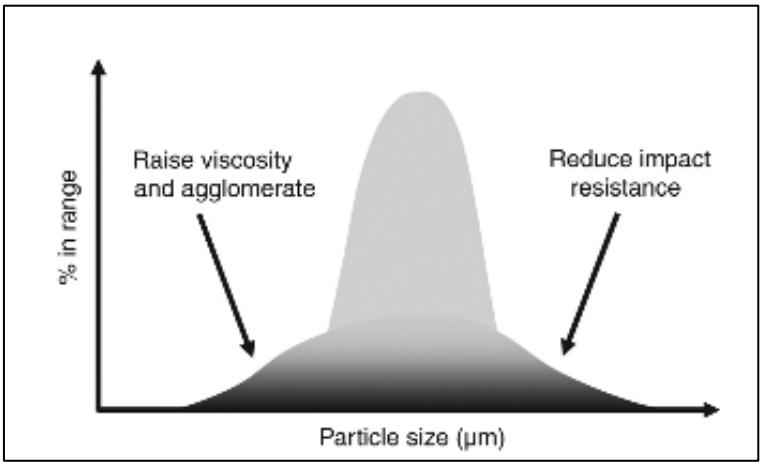


FIGURE 7. Distribution of particle size and its effect on mechanical properties (adapted from DeArmitt 2017, 517-532.)

# 3 RECENT DEVELOPMENTS IN FUSED DEPOSITION MODELING OF POLYMER COMPOSITES

Although the FDM technique with polymer material can be used in wide applications, the mechanical properties of the printed parts are very low resulting in breakage and failure to the produced structure. To significantly improve the mechanical properties of the FDM end product, reinforcement of polymer material and process parameter optimization has been introduced in the last decade. (Zhong et al. 2001; Shofner et al. 2003; Torrado Perez, Roberson & Wicker 2014; Tekinalp, Kunc, Velez-Garcia, Duty, Love, Naskar, Blue & Ozcan 2014; Hwang, Reyes, Moon, Rumpf & Kim 2015; Li et al. 2016, Le Duigou, Castro, Bevan & Martin 2016; Wang et al. 2016; Sezer and Eren 2019; Sodeifian et al. 2019; Camargo et al. 2019; Heidari-Rarani et al. 2019.)

In this chapter, recent research developments on FDM of fiber-reinforced composites and their effect on the mechanical properties are reviewed and collected. Process parameters and their effect on the FDM processed parts are also noted. The chapter is sub-categorized by the polymer matrix of ABS, PLA, PE, and PP which were used in the collected research papers. The processing information of each experiment is tabulated and the results regarding the mechanical properties are discussed in the text. Generally, in all experiments, polymer and fiber materials were firstly compounded and made into filaments. Subsequently, these filaments were used as FDM material for producing test specimens that were used for testing mechanical properties.

## 3.1 Composite based on acrylonitrile butadiene styrene (ABS)

In this sub-chapter, recent developments of composite based on ABS are collected. The process methods and parameters are tabulated and their effect are described in the text.

### 3.1.1 Short carbon fiber (CF)

Tekinalp et al. analyzed the mechanical properties when ABS is reinforced with short carbon fiber (CF). The objective of this research was to study the effect of fiber loading, fiber length, and distribution of

carbon fiber on the tensile properties of compression molded (CM) and FDM printed polymer composites. Additional process condition is shown in Table 4. (Tekinalp et al. 2014.)

TABLE 4. Process information of ABS polymer reinforced with CF (adapted from Tekinalp et al. 2014.)

| | |
|---|---|
| **Parameter** | Infill of CF: 0, 10, 20, 30, 40 wt.%<br>Method of printing: CM, FDM |
| **Material** | ABS (GP35-ABS-NT)<br>CF (epoxy-based sizing of 3.2 mm) |
| **Process equipment** | Intelli-Torque Plasti-Corder Brabender mixer, FDM unit (Solidoodle 3) |
| **Experiment process** | Compounding:<br>ABS and CF compounded with a Brabender mixer at 220 ℃<br>Average mixing time (including feeding time): 13 min<br>Different infill mixtures prepared<br>Neat ABS run through the same condition<br>Mixture extruded at 220 with plunger-type batch extrusion unit<br>Test specimen production:<br>CM: slit-shaped die<br>FDM: cylindrical die (diameter: 1.75 mm)<br>Test specimen dimension: ASTM D638 type-V dog-bone |
| **Nozzle temperature in °C** | 205 |
| **Bed temperature in °C** | 85 |
| **Nozzle diameter in mm** | 0.5 |
| **Layer height in mm** | 0.2 |

The tensile strength of the FDM printed composites increased with increasing fiber content by reaching the highest strength of approximately 65 MPa at a fiber loading of 40 wt.%. At the fiber loading of 30 wt.% and 40 wt.% the strength seems to be reaching a plateau. This phenomenon was explained based on the decrease in average fiber length at higher fiber loading due to fiber breakage occurred during the composite manufacturing process. These phenomena were more commonly shown in the FDM printing method compared to the CM method due to additional fiber breakage occurring when the melt pass through the nozzle. This resulted in higher tensile strength of CM samples compared to the FDM printing method with a value of approximately 75 MPa at fiber loading of 40 wt.%. (Tekinalp et al. 2014.)

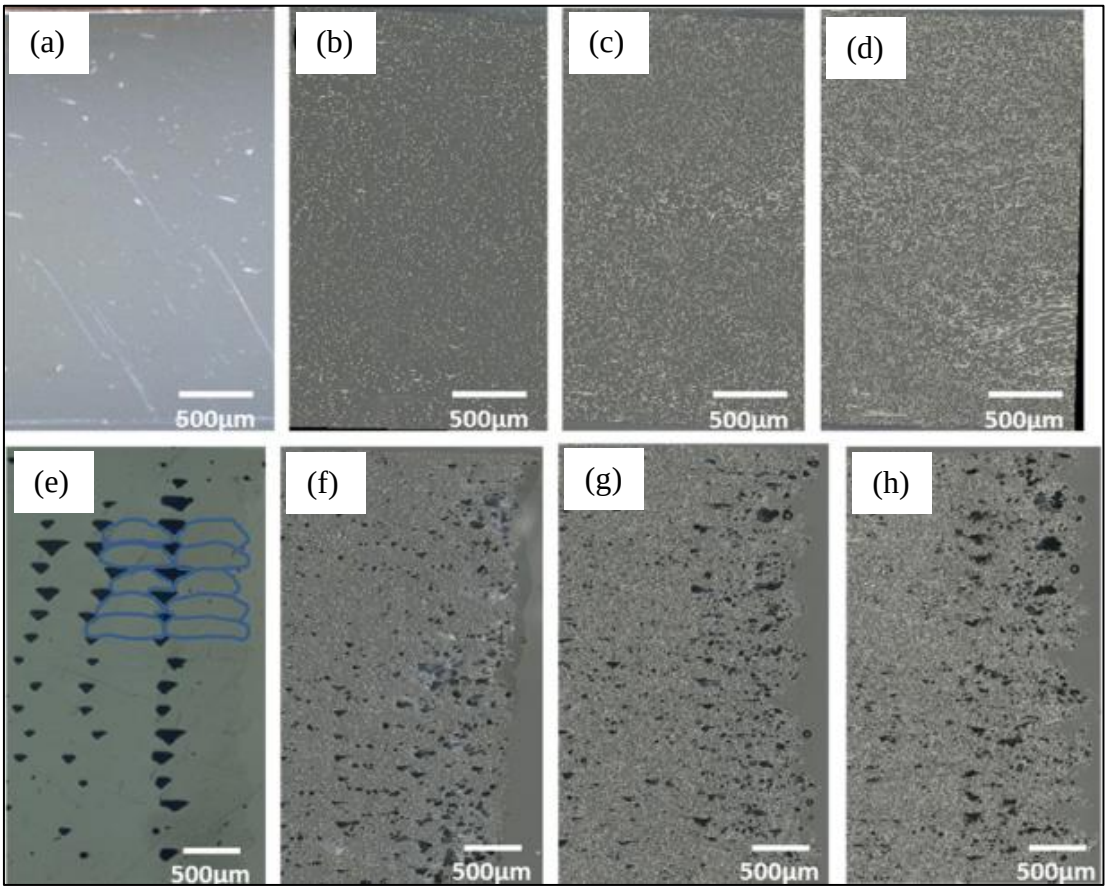


FIGURE 8. SEM micrographs of polished cross section of test specimen slices of (a) CM neat ABS (b) CM 10 wt.% CF, (c) CM 20 wt.% CF, (d) CM 30 wt.% CF, (e) FDM neat-ABS, (f) FDM 10 wt.% CF, (g) FDM 20 wt.% CF and (h) FDM 30 wt.% CF (adapted from Tekinalp et al. 2014, 147.)

Microscopy images of the polished cross-section of the dogbone test specimens are shown in Figure 8. CM test specimens showed no visible voids however, FDM samples showed a significant fraction of voids. The neat ABS FDM printed samples contained inter-bead pores lined up in triangle channels formed by the layering printing process. By the inclusion of CF, the size of inter-bead voids seems to be decreasing however, the inner-bead voids began to form. The voids inside the beads tend to create stress concentration points resulting in lower tensile strength. Therefore, FDM test specimens resulted in lower tensile strength compared to CM samples. The study concluded the need for modification and optimization of the melt mixing process to minimize fiber breakage and modification of the FDM process to minimize inner-pore formation for better attachment of fiber and polymer. (Tekinalp et al. 2014.)

### 3.1.2 Multiwall carbon nanotube (MWCNT)

Sezer and Eren demonstrated FDM printing with composites of the ABS matrix reinforced with a multiwall carbon nanotube (MWCNT). The study aimed to analyze the effect of fiber infill percentage and printing angle on mechanical and electrical properties such as tensile strength, ductility, and modulus. In this study, the fiber distribution was improved by adding a twin-screw micro compounder with a mixing chamber at the beginning of the process. Further process conditions are mentioned in Table 5.

TABLE 5. Process information of ABS reinforced with MWCNT (adapted from Sezer & Eren 2019.)

| | |
|---|---|
| **Parameter** | Infill of MWCNT: 0, 1, 3, 5, 7, 10 wt.%<br>Printing angle: [90°, 0°] [-45°, 45°] |
| **Material** | MWCNT (9.5 nm average diameter,1.5 $\mu$m average length, 250-300 $m^2/g$ surface area, 90 % Carbon purity via catalytic carbon vapor deposition (CCVD)<br>ABS 1.05 $g/cm^3$ |
| **Process equipment** | Twin-screw micro compounder extruder, Single screw extruder (Wellzoom C) |
| **Experiment process** | Compounding:<br>Raw materials mixed in the twin-screw extruder for a homogeneous distribution<br>Extruded and granulated into small pellets<br>Screw speed: 100 rpm, Mixing time: 5 min, Temperature: 240 °C<br>Filament production:<br>Pellets fed into the single extruder and transformed out as a filament form of diameter 1.7 mm<br>Composite preheated: 220 °C, extruded: 235 °C, extrusion rate: 2000-2200 mm/min<br>Test specimen production:<br>Test specimen dimension: ASTM D412 A<br>Printing angle: [90°, 0°]: Extrusion road contains mostly 0° and 90° are at the connecting curves, [-45°, 45°]: cross extrusion road of 45°and 45° by one layer to another |
| **Nozzle temperature in °C** | 240-245 |
| **Bed temperature in °C** | 110 |
| **Nozzle diameter in mm** | 0.4 |
| **Layer height in mm** | 0.2 |
| **Printing speed in mm/min** | 1800 |

Increase of MWCNT infill improved the tensile strength, Young's modulus and electrical properties, however, showed a decrease for elongation at yield for both printing angles. The printing angle [90°, 0°]

provided continuity of extrude paths leading to significantly better tensile and electrical properties compared to discontinuous cross layers resulted from [-45°, 45]. At the printing angle [90°, 0°], a slight decrease of tensile strength was shown at infill of 1 wt.% MWCNT being considered a ductile to the brittle transition zone. From 1 wt.% MWCNT infill and onwards, samples showed brittle behavior with decreased elongation. However, the tensile strength showed continuous increase until the optimum value (≈ 67 MPa) was reached at 7 wt.% of MWCNT which had 288 % higher strength value than the neat ABS (≈ 44 MPa). This was believed resulted by the uniaxial loading along the MWCNT in [90°, 0°]. In addition, a homogeneous distribution of MWCNT can be seen in Figure 9. From 7 wt.% MWCNT loading and further tensile strength started to decrease with a large error range. The bunching of nanoparticles at high fiber loading percentage resulted to be the reason. The printing angle of [-45°, 45] showed similar results. Melt flow index (MFI) had a significant decrease as the fiber loading increased, resulting in 164 times lower MFI value at 10 wt.% MWCNT compared to neat ABS. Low MFI value caused difficulty at extrusion bringing filament breakage and nozzle clogging. (Sezer & Eren 2019.)

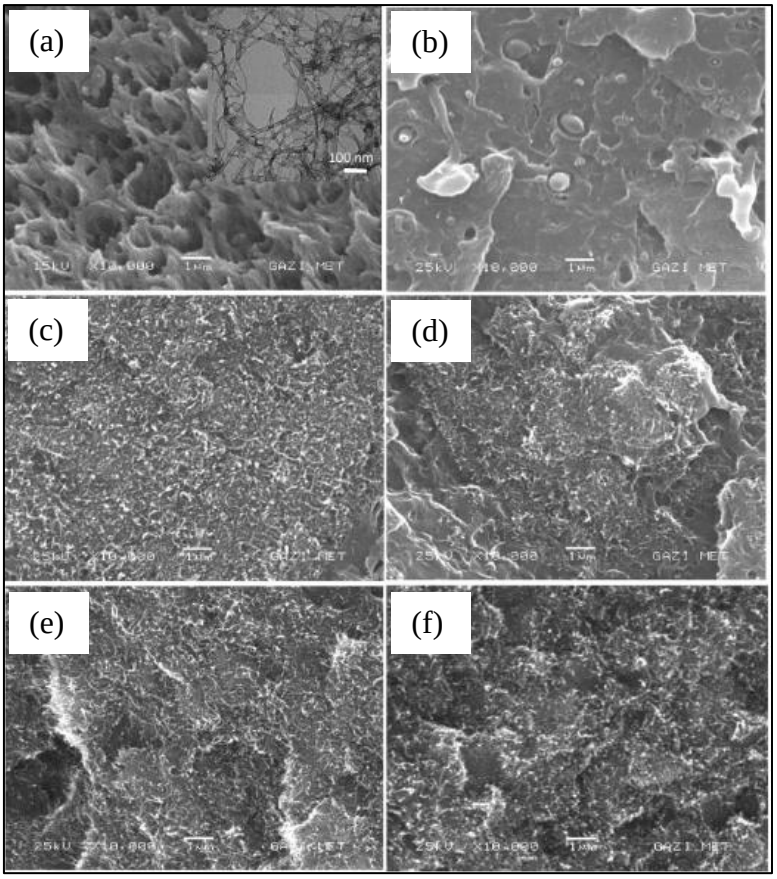


FIGURE 9. SEM micrographs of tensile test fracture surface of dog bone samples of (a) neat ABS and raw MWCNT at right corner, (b) MWCNT 1 wt.%, (c) MWCNT 3 wt.%, (d) MWCNT 5 wt.%, (e) MWCNT 7 wt.%, (f) MWCNT 10 wt.%. (adapted from Sezer & Eren 2019.)

### 3.1.3 Vapor grown carbon fiber (VGCF)

Another carbon fiber reinforced experiment was done by Shofner et al. The composite was reinforced with a continuous fiber of vapor grown carbon fibers (VGCF). The VGCF can be seen in Figure 10. The studied parameters were the loading of VGCF, the printing angles. Two different ABS matrix from Magnum213 and P400 were tested which brought similar results. (Shofner et al. 2003.) Further process information is shown in Table 6.

TABLE 6. Process information of ABS reinforced with VGCF (adapted from Shofner et al. 2003.)

| | |
|---|---|
| **Parameter** | Addition of VGCF 0, 10 wt.%<br>Different ABS matrix: Magnum213, P400<br>Sample shape: straight bar, dog bone shape, ASTM D638 Type V dog-bone<br>Printing angle:<br>-Straight bar: [0°, 90°], [90°, 0°] [-45°, 45°]<br>-Dog-bone: [10°, 90°]<br>-ASTM D638 type V dog-bone [0°, 0°] |
| **Material** | VGCF Pelletized form, average diameter: 100 nm, length: order of 100 μm<br>ABS (MAGNUM 213, P400) |
| **Process equipment** | Banbury mixer (HAAKE Polylab), Single-screw extruder, FDM machine (Stratasys FDM 1600 modeler) |
| **Experiment process** | Pretreatment:<br>Removal of amorphous carbon particles and catalyst of VGCF<br>Compounding:<br>ABS compounded with VGCF to achieve a homogeneous dispersion of 10 wt.% VGCF<br>Mixed material was compressed molded and made into sheets<br>Compressed sheets granulated<br>Filament production:<br>Granulate materials fed to the single-screw extruder at a rate of 5 rpm<br>Filament extruded from the single-screw extruder spooled by hand to FDM reel (maintain the constant diameter of filament) nominal diameter: 1.7 mm, length of 20 m each spool<br>Test specimens production:<br>Spools used in FDM machine to produce different sample shapes<br>Blank ABS filaments extruded by the same method<br>First angle: alignment of the top layer (last built)<br>Example: at [0°, 90°] from top to bottom the layer order is 0°, 90°,…0°.<br>Straight bar specimen: 11 layers, dog-bone specimen: 6 layers, ASTM D638 Type V Dog bone specimen: 5 layers. |

During the tensile testing, all the straight bar samples broke due to grip fracture. Therefore, the tests were conducted with dog bone shape samples according to ASTM D638 Type V. This solved the problems occurring from fractures at straight bar samples grip region and improved the interlayer and

intralayer fusion for maximizing part strength. The ASTM D638 Type V sample shape showed the highest tensile strength compared to others. All three sample shapes showed improvement on stiffness and strength with addition of VGCF, resulting in reduce of swelling of material during the extrusion process, however it showed a drastic decrease in elongation at failure leading brittleness to the final product. For dog-bone shape samples, 10 wt.% VGCF composite samples showed a higher tensile strength of approximately 24.5 MPa compared to neat ABS (≈19 MPa). ASTM D638 Type V samples, 10 wt.% VGCF composite sample (≈ 37.4 MPa) showed 39-60 % higher tensile strength compared to neat ABS (≈ 26.5 MPa). Due to the grip fractures for straight bar samples, the strength was not effectively measured. However, the layer alignments were checked to compare the printing angle effect. Printing angle of [45°, 45°] was assumed with a better tensile strength of 15 % than angles of [0°, 90°] and [90°, 0°] due to lower intralayer voids at the cross-section parts. Shofner et al. concluded, further fiber treatments could improve the fiber and matrix adhesion leading to better ductility and mechanical properties of printed parts. (Shofner et al. 2003.)

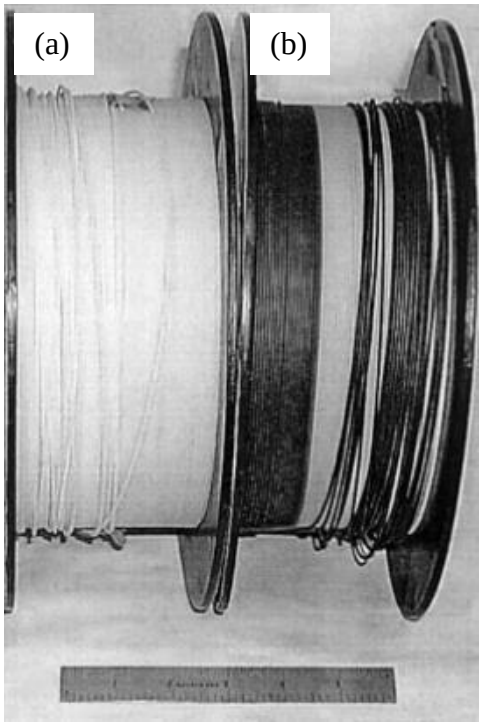


FIGURE 10. Continuous filament spools extruded by single-screw extruder (a) filaments of blank ABS filament (b) filaments of 10 wt.% VGCF (adapted from Shofner et al. 2003, 3081–3090.)

### 3.1.4 Glass fiber/ linear low-density polyethylene/ ethylene-ethyl-acrylate/ hydrogenated buna-N

Zhong et al. conducted a study to improve material properties of the ABS matrix by the addition of short glass fiber (GF), linear low-density polyethylene (LLDPE), hydrogenated Buna-N or ethylene-ethyl-acrylate (EEA). (Zhong et al. 2001.) Further process information can be seen in Table 7.

TABLE 7. Process information of ABS reinforced with GF, LLDPE, Hydrogenated Buna-N, EEA (adapted from Zhong et al. 2001.)

| | |
|---|---|
| **Parameter** | Infill of GF: 15, 20, 25, 30wt.%<br>Infill of LLDPE: 10, 30wt.%<br>Addition of hydrogenated Buna-N or EEA |
| **Material** | ABS (Qimei-757)<br>Short glass-reinforced ABS (GFABS-30)<br>Linear low-density polyethylene (LLDPE)<br>Hydrogenated Buna-N (0209)<br>Ethylene-ethyl-acrylate (EEA) |
| **Process equipment** | Twin-screw extruder (TE-34, Screw diameter: 34 mm, L/D: 34), Single-screw extruder (diameter: 30 mm, length: 800 mm), FDM machine (MEM-250) |
| **Experiment process** | Compounding:<br>Raw materials mixed in the twin-screw extruder (improve mixture distribution)<br>Extruded and granulated into small pellets<br>Filament production:<br>Pellets fed into the single extruder and transformed out as a filament form (diameter: 1.75-1.90 mm)<br>Test specimens production:<br>Printing angle of FDM: 90°, test specimen dimensions: 50·50·100 $mm^3$, 100·100·90 $mm^3$ |
| **Nozzle temperature in °C** | 250 |
| **Bed temperature in °C** | 60 |
| **Layer height in mm** | 1.75-1.9 |
| **Rotation speed in r/min** | 140 |

Addition of GF fiber to ABS decreased the adhesive strength between the layers, however with increase of infill, GF had better chance to bridge between the layers before solidifying. In result, 30 wt.% GF reinforced ABS samples showed a significant increase in strength, softening temperature, and heat distortion temperature leading in decrease of shrinkage and improved surface rigidity compared to neat ABS samples. However, the toughness was reduced due to its melts becoming brittle after being extruded and cooled at room temperature. Attempted on improving the toughness was done by producing lowered GF loading specimens (15, 20, and 25 wt.%) however, similar toughness was shown with 30 wt.% GF-

ABS and this method was still not feasible. LLDPE (10 and 30 wt.%) as a plasticizer was added to 30 wt.% GF-ABS. These specimens showed improvement in flexibility and ductility, indicating an effective toughness agent. However, LLDPE above 30 wt.% brought extensive phase separation between ABS and LLDPE. As a result, hydrogenated buna-N was added as a compatibilizer between ABS and LLDPE. The addition of 10 g of hydrogenated buna-N to GF 13.2 wt.%-100 g LLDPE resulted in a tensile strength increase from 38.93 MPa to 52.37 MPa. The acrylonitrile and butadiene groups contained in Buna-N of the hydrogenated buna-N are similar to the ABS structure and the hydrogen buna-N main chain structure -$CH_2$- is structurally similar to LLDPE. The separation of filaments disappeared, and the toughness and filament appearance improved even with the further addition of GF (GF18 wt.%-100 g LLDPE 10g hydrogenated Buna-N: 58.6 MPa). In Figure 11, SEM micrographs of specimens with and without hydrogenated buna-N can be seen. The addition of Ethylene-ethyl-acrylate (EEA) did not result in any obvious improvement in the properties. (Zhong et al. 2001.)

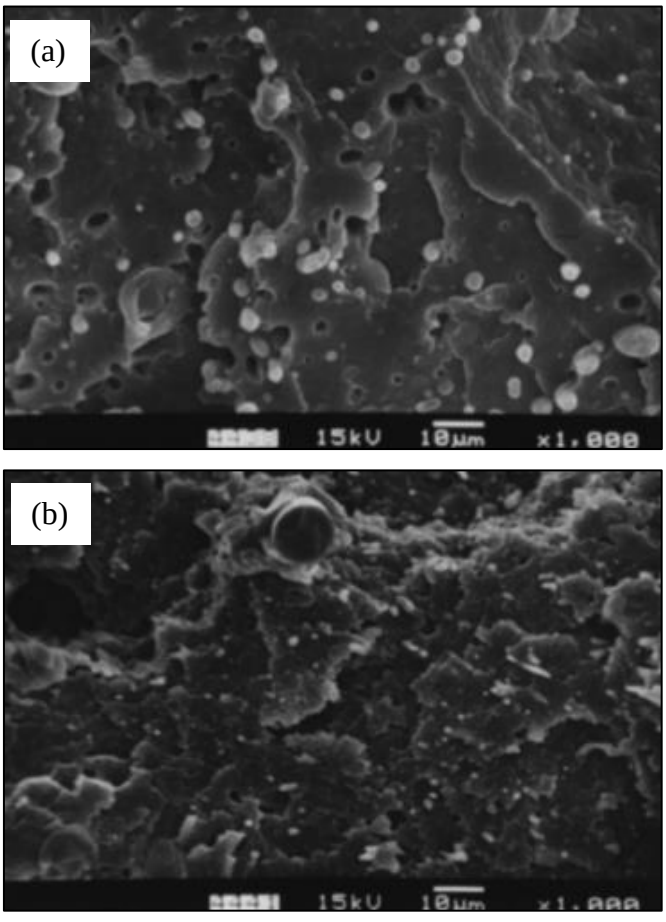


FIGURE 11. SEM micrograph of (a) sample of GF 13.2 wt.% without hydrogenated buna-N (GFABS-30 440 g, ABS 440 g, LLDPE 100 g, PE 20 g), (b) sample of GF 13.2 wt.% with hydrogenated buna-N (GFABS-30 440 g, ABS 430 g, LLDPE 100 g, PE 20 g, hydrogenated buna-N 10 g) (adapted from Zhong et al.2001.)

### 3.1.5 Copper (Cu)/ iron (Fe)

Hwang et al. carried an experiment with copper (Cu) and iron (Fe) as a reinforcement filler to the ABS matrix. The objective of the study was to analyze the mechanical properties derived from different printing temperature, fill density, and infill percentage of copper and iron. (Hwang et al., 2015.) The process information can be seen in Table 8.

TABLE 8. Process information of ABS reinforced with Cu or Fe (adapted from Hwang et al., 2015.)

| | |
|---|---|
| **Parameter** | Infill of metal powder: copper 10, 30 wt.%, iron 10, 30, 40 wt.%<br>Printing temperature: 190, 200, 210, 220 ℃<br>Fill density: 20, 40, 60, 80 % |
| **Material** | Copper (Size: less than 24μm-625 mesh, 99 %)<br>Iron (Size: 43 μm-325 mesh, 98 %) |
| **Process equipment** | Filament extruder (Filastruder) diameter: 1.75 mm, FDM 3D printer (NP-Mendel) |
| **Experiment process** | Compounding:<br>Copper and iron powders were mixed with ABS<br>Metal and ABS mixture formed in pellets<br>Filament production:<br>Pellets extruded by filament extruder<br>Test specimens production:<br>Test specimen dimension: ASTM D638 dog-bone<br>Printing angle: not mentioned |
| **Nozzle temperature in °C** | 190, 200, 210, 220 |
| **Bed temperature in °C** | 120 |
| **Rate in /min** | 10 |
| **Layer height in mm** | 1-2 |
| **Nozzle diameter in mm** | 1.75 |

The increase of printing temperature from 190 to 220 ℃ resulted in an increase of tensile strain (≈3.8 to 8 %,), tensile strength (≈25 to 53 MPa), volumetric flow rate (≈$1.82 \cdot 10^{-9}$ to $3.47 \cdot 10^{-9}$ $m^3/s$), and decrease of viscosity (≈3.9 to 2.2 cP) of ABS specimens. These values lead to assumptions of stronger layer adhesions with increase of temperature. The tensile strength and strain decreased stepwise by higher infill of Cu (10 and 30 wt.%: [42, 26.5 MPa], [5.4, 3.3 %]) and Fe (10, 30 and 40 wt.%: [43.4, 40.6, 36.2 MPa], [6.1, 5.1, 4.5 %]). This phenomenon was explained based on the lower binding between layers derived from higher void content at increase of Cu infill. In Figure 12, the enlarged void content can be seen with higher Cu infill. The Young's modulus increased with a higher infill of Cu (10wt.%: 930.2 MPa) and Fe (10 and 30 wt.%: 906.1, 978.5 MPa) however, showed a slight decrease at the highest infill percentages (Cu: 915.9, Fe: 958.2 MPa). Increasing the fill density resulted in better tensile strength but

no significant difference in the strain. Fill density of 60 % had the highest tensile strength (≈34 MPa) with the highest ductility. The addition of copper particles improved the thermal conductivity (Cu 0 wt.%: 0.646, Cu 50 wt.%: 0.912 W/mK). When comparing neat ABS and 50 wt.% Cu-ABS, an improvement of 41 % is shown. Hwang et al. mentioned the enhanced thermal conductivity by the addition of metal particles leads its opportunities in the field of large-scale 3D electromagnetic structures such as antennas. (Hwang et al., 2015.)

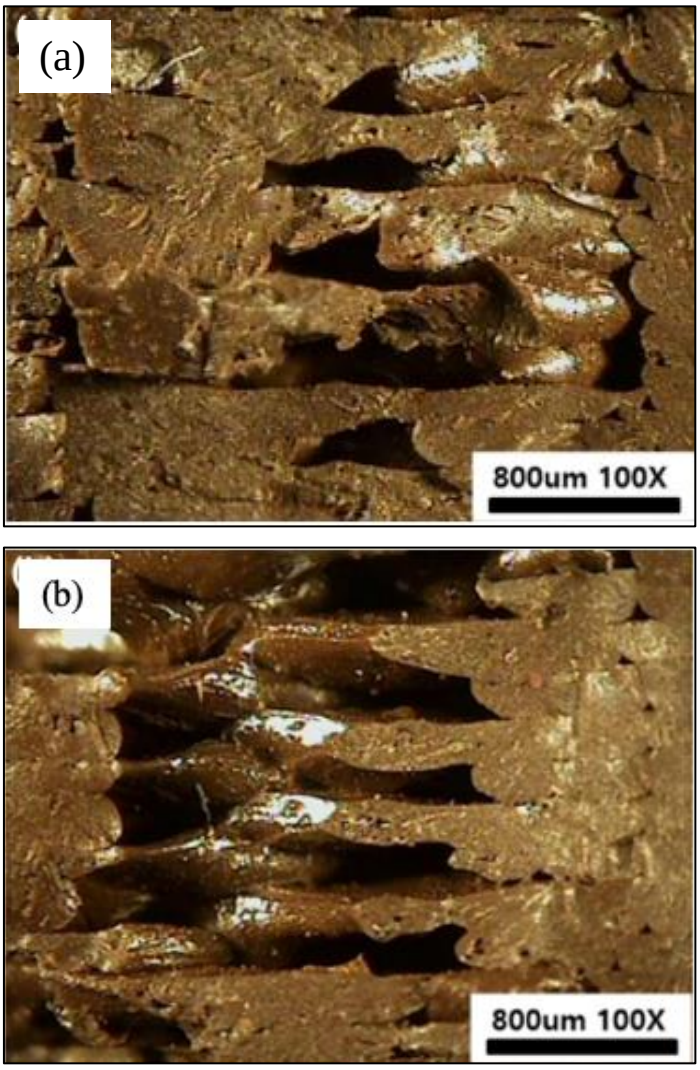


FIGURE 12. SEM micrographs of cut-section of specimens of (a) ABS-Cu10 wt.% (b) ABS-Cu30 wt.% (adapted from Hwang et al. 2015.)

### 3.1.6 Jute fiber/ Titanium dioxide ($TiO_2$)/ Thermoplastic elastomer (TPE)

Torrado et al. experimented with jute fiber, thermoplastic elastomer (TPE), and titanium dioxide ($TiO_2$) to reinforce the ABS matrix. The research aimed to study the mechanical properties of composites produced with different additives and build orientation. (Torrado Perez et al., 2014.) Detailed process information is shown in Table 9.

TABLE 9. Process information of ABS reinforced with jute fiber, $TiO_2$, TPE (adapted from Torrado Perez et al. 2014.)

| | |
|---|---|
| **Parameter** | Types of additive: Jute fiber 5 wt.%, titanium dioxide $TiO_2$ 5 wt.%, TPE 5 wt.%<br>Build orientation: vertical 90°, horizontal 0° |
| **Material** | ABS, Jute fiber, $TiO_2$, thermoplastic elastomer (TPE) |
| **Process equipment** | Twin-screw extruder/compounder (ZK 25T), 3D printer (MakerBot Replicator, Diameter: 1.77 mm) |
| **Experiment process** | Compounding:<br>Raw materials mixed in a twin-screw extruder<br>Extruded and granulated into small pellets. Screw speed: 100rpm total mixing time: 5min<br>Filament production:<br>Pellets fed into the single extruder and transformed out as a filament form<br>Test specimen production:<br>Test specimen dimension: ASTM 638, type V |
| **Nozzle temperature in °C** | 230 |
| **Bed temperature in °C** | - |
| **Layer height in mm** | 0.27 |
| **Nozzle diameter in mm** | 0.4 |
| **Feed rate in mm/s** | 40 |

In general, test specimens printed in 0° direction presented better mechanical strength compared to 90° printed parts. This was assumed by the higher inner-void content of 90° printed parts which leads to lower-layer bonding. Further morphological properties of each test specimen can be seen in Figure 13. Polymer filled with 5 wt.% $TiO_2$ showed an increase of tensile strength in both the printing direction of 0° (32.2 MPa) and 90° (18.4 MPa) by 13.2 % and 30 % compared to pure ABS (0°: 28.5, 90°: 14.1 MPa). The $TiO_2$ restricted the polymer macromolecules movement which resulted in higher tensile strength however, indicated brittleness and low roughness to the polymer composite. The elastic property of TPE gives higher freedom to polymer macromolecules to slide over each other. This resulted in better stiffness to the TPE composite leading to 90° printing direction (9.1 %) withstand 31 % more strain

compared to pure ABS (1.5 %), and printing direction 0° (2.1 %) with a comparable value to the pure ABS (2.2 %). However, tensile strength (0°: 24, 90°: 9.1 MPa) reduced by both printing directions compared to pure ABS. Despite the lower tensile strength from TPE reinforced composite, it resulted in final surface improvement and reduction of warping by the printing process. Jute fiber-reinforced composite at a fiber loading of 5 wt.%, (0°: 25.9, 90°: 12.9 MPa) reduced the tensile strength from both printing directions compared to pure ABS. At the printing direction of 0° (23.6 MPa) jute fiber composite showed 28 % increase and at printing direction 90°, 31 % decrease of fracture strength compared to pure ABS (0°: 18.4 MPa). This was assumed from printing angle and the inner-void and by-product formation resulted by the combustion gas generation by the decomposition of jute fiber (180 ℃) at nozzle extrusion. On the other hand, jute-ABS composite showed a decrease in warping and the highest value of roughness of four compared materials. (Torrado Perez et al. 2014.)

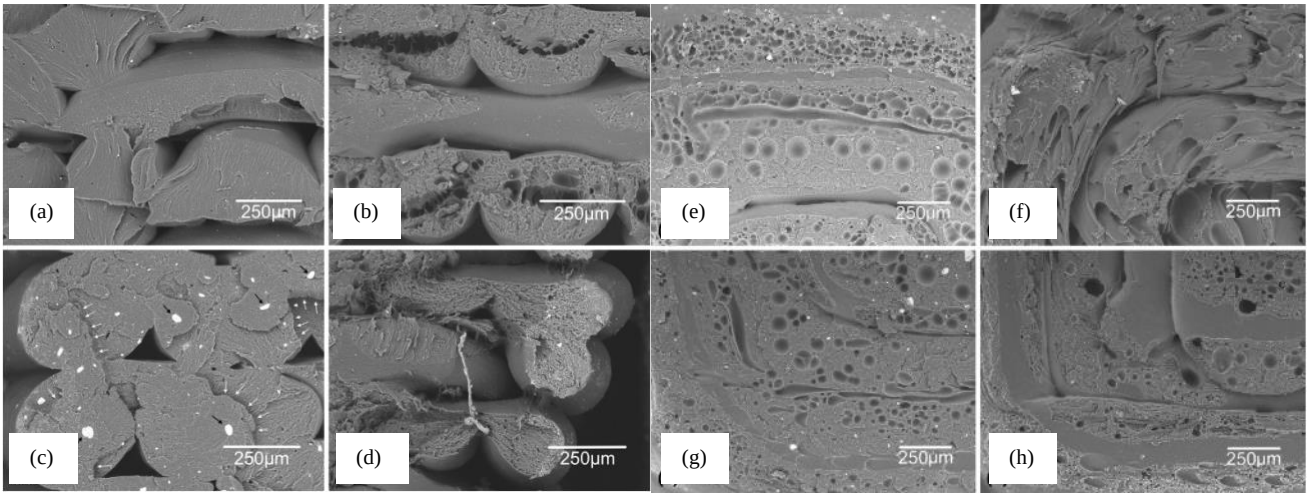


FIGURE 13. SEM micrographs of fracture surfaces of 0° sample (a) ABS (b) ABS-jute fiber (c) ABS-$TiO_2$ (d) ABS-TPE and 90° samples of (e) ABS (f) ABS-jute fiber (g) ABS- $TiO_2$ (h) ABS-TPE (adapted from Torrado Perez et al., 2014.)

### 3.2 Composite based on polylactic acid (PLA)

In this sub-chapter, recent developments of composite based on PLA are collected. The process methods and parameters are tabulated and their effect are described in the text.

### 3.2.1 Graphene

Camargo et al. studied the mechanical properties such as tensile strength, flexural strength, and the impact energy of graphene reinforced PLA fabricated parts. The effect of different graphene infill percentage and printed layer height on mechanical properties were tested. (Camargo et al. 2019.) Further process information can be seen in Table 10.

TABLE 10. Process information of PLA reinforced with graphene (adapted from Camargo et al. 2019.)

| | |
|---|---|
| **Parameter** | Infill percentage: 10, 22, 50, 78, 89 wt.%<br>Layer height in s :0.1, 0.13, 0.2, 0.27, 0.3 mm |
| **Material** | PLA-graphene |
| **Process equipment** | 3D printer (Delta) printing capacity: 135·135·270 $mm^3$ (X · Y · Z) |
| **Experiment process** | Filament production:<br>PLA-graphene filament form material fed to FDM machine (diameter 1.75 mm)<br>Filament and prepared samples kept in airtight packaging at controlled temperature<br>Test specimen production:<br>Tensile specimen dimension: ASTM D638-14<br>Flexural specimen dimension: ASTM D790-17<br>Impact specimen dimension: ASTM D256-10<br>Raster angle: 45°<br>Samples of PLA/G10 wt.% (s=0.2), PLA/G22 wt.% (s=0.13, 0.27), PLA/G50 wt.% (s=0.1, 0.2, 0.3), PLA/G78 wt.%(s=0.13, 0.27), PLA/G 89 wt.% (s=0.2) |
| **Nozzle temperature in °C** | 200 |
| **Bed temperature in °C** | 60 |
| **Layer height in mm** | 0.13-0.27 |
| **Nozzle diameter in mm** | 0.4 |
| **Printing speed in mm/min** | 3000 |

Previous studies concluded that PLA specimen shows an increase of tensile strength as layer height decrease (Tymrak, Kreiger, and Pearce 2014; Chacón, Caminero, García-Plaza & Núñez 2017). However, graphene reinforced PLA showed different results. Tensile strength and flexural strength were significantly increased with an increase of layer height and infill. During the experiment, the highest tensile strength of 33.7 MPa and flexural strength of 60.9 MPa were brought by a layer height of 0.27 mm and infill of 78 wt.%. Using a theoretical model equation, a maximum tensile strength value of 37.9

MPa and flexural strength of 68.5 MPa were brought by 0.3 mm of layer height and 85 wt.% of infill. (Camargo et al. 2019.)

### 3.2.2 Continuous carbon fiber reinforcement (CCFR)

Heidari-Rarani et al. developed an innovative extruder for fabricating continuous fiber-reinforced thermoplastic composites. In Figure 14, the designed extruder and the scheme of the general printing process can be seen. With the manufactured extruder, samples of pure PLA and continuous carbon fiber reinforced (CCFR) PLA were fabricated with different process conditions, and the mechanical properties were studied. The carbon fiber rovings used as the CCFR material were surface treated with polyvinyl alcohol (PVA) dissolved water to modify the CCFR surface and enhance the matrix-fiber bonding. (Heidari-Rarani et al. 2019.) Further process parameters can be seen in Table 11.

TABLE 11. Process information of PLA reinforced with CCFR (adapted from Heidari-Rarani et al. 2019.)

| **Parameter** | Addition of CCFR |
|---|---|
| **Material** | PLA, CCFR |
| **Process equipment** | FDM machine (MarkOne, newly designed extruder), 3D model software (SolidWorks) |
| **Experiment process** | Preprocessing:<br>Carbon fiber roving is impregnated in 400 g polyvinyl alcohol (PVA) dissolved in 2 L water. (1 h 60 °C): change to a compatible sizing<br>Dried at room temperature to remove extra PVA<br>Test specimen production:<br>Polymer filament (diameter: 1.75 mm) and fiber enters different entry of the extruder<br>Printing direction: longitude direction = 0°<br>Test specimen dimension: ASTM D790, ASTM D638, ASTM D3039<br>A cooling fan located on the extruder to reduce cooling time: avoid fiber-matrix debonding |
| **Nozzle temperature in °C** | Pure: 210, Composite: 215 |
| **Bed temperature in °C** | - (atmosphere temperature) |
| **Nozzle diameter in mm** | Pure: 0.4, Composite: 2 |
| **Layer height in mm** | Tensile specimen: pure: 0.3, composite: 0.5 adjusted 1 printed, bending specimen sample: 3.2 |
| **Printing speed in mm/s** | Pure: 20, Composite: 5 |

The tensile and bonding properties of each prepared sample were analyzed. CCFR reinforced PLA showed higher tensile strength (61.4 MPa), tensile modulus (8.28 GPa), bending strength (152.1 MPa) and bending modulus (13.42 GPa) by 36 %, 208 %, 109 % and 367 % compared to pure PLA (44.86 MPa, 2.69 GPa, 72.76 MPa, 2.87 GPa). Also, the morphological analysis concluded the surface treatment of PVA was very effective. (Heidari-Rarani et al. 2019.)

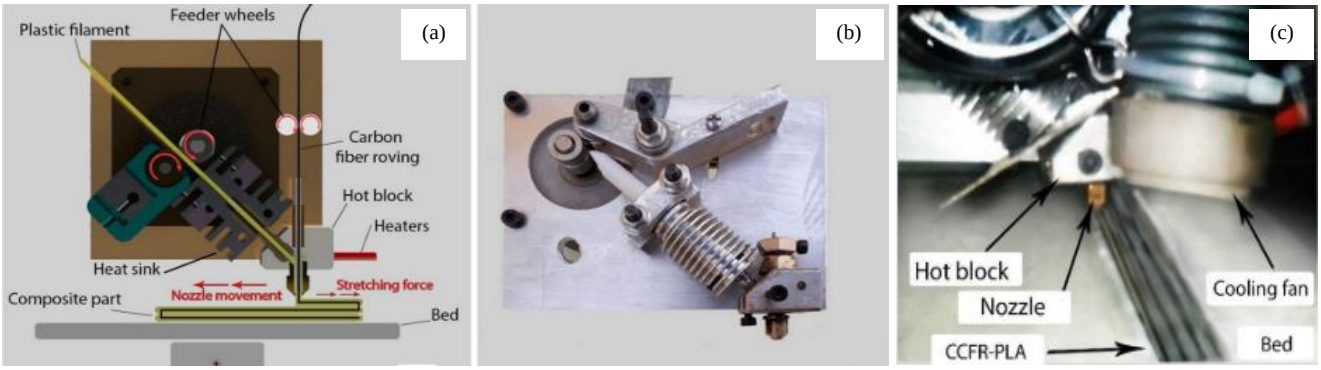


FIGURE 14. (a) a novel scheme of the fabricating process (b) developed innovative extruder (c) fabricating process with an operating cooling fan (adapted from Heidari-Rarani et al. 2019.)

Li et al. conducted another experiment with CCFR. The type of CCFR used in this experiment was a 1000 single carbon fiber bundle (HtA40 H13). The focus of this research was to compare the mechanical properties of three test specimens produced of pure PLA, processed carbon fiber bundle-PLA, and non-processed carbon fiber bundle-PLA. The processed carbon bundle was sized in aqueous PLA agents for surface modification before the FDM printing process. (Li et al. 2016.) The scheme of the fabrication process can be seen in Figure 15 and further process information is described in Table 12.

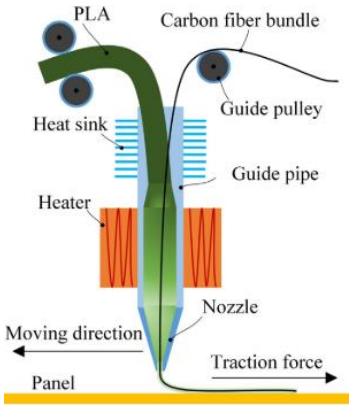


FIGURE 15. The scheme of fabrication of continuous carbon fiber reinforced PLA (adapted from Li et al. 2016.)

TABLE 12. Process information of PLA reinforced with CCFR (adapted from Li et al. 2016.)

| **Parameter** | Process of carbon fiber: Processed, non-processed carbon fiber bundle |
|---|---|
| **Material** | CCFR bundle (1000 single carbon fibers, HtA40 H13)<br>Polylactic acid resin 98 %<br>Methylene dichloride solution |
| **Process equipment** | Modified screw-type extruder (Wellzoom-B), Emulsification machine (DE-100LB) |
| **Experiment process** | Filament production:<br>Polymer matrix: PLA wire rod is produced with screw-type extruder<br>Continuous fiber: Aqueous PLA sizing agent modify the surface condition of carbon fiber<br>Test specimen production:<br>Continuous PLA wire and carbon fiber bundle contact at the guide pipe and heated at melt temperature before extrusion at the nozzle<br>(heat sink at the guide pipe entrance to ensure solid state of PLA material)<br>Printing direction: longitude, printing path starts from inside to outside clockwise |
| **Layer height in mm** | 2.3 |

Non-processed carbon fiber bundle-PLA samples seen in Figure16 (a) shows numerous voids between carbon fibers. Processed carbon fiber bundle-PLA samples (b) shows homogeneous distribution of PLA between carbon bundles and an almost void-free structure. Fracture surface after the tensile test of both processed and non-processed carbon fiber bundles showed a different result. The non-processed sample had very little PLA resin covering the fractured carbon surface (c) and on the other hand, processed sample (d) resulted in a plentiful generous amount of PLA resin around the cracked carbon fibers. These results explain the significant difference of flexure strength between the samples of modified and non-modified CCFR samples with values of 59 MPa and 156 MPa. Furthermore, the tensile strength of the modified CCFR-PLA sample showed the highest value of 91 MPa followed by 28 MPa and 80 MPa for the pure PLA and non-modified CCFR-PLA samples. Li et al. concluded that the surface modification of continuous carbon fiber increased the interfacial bond and strength of the layers resulting in better mechanical properties. (Li et al. 2016.)

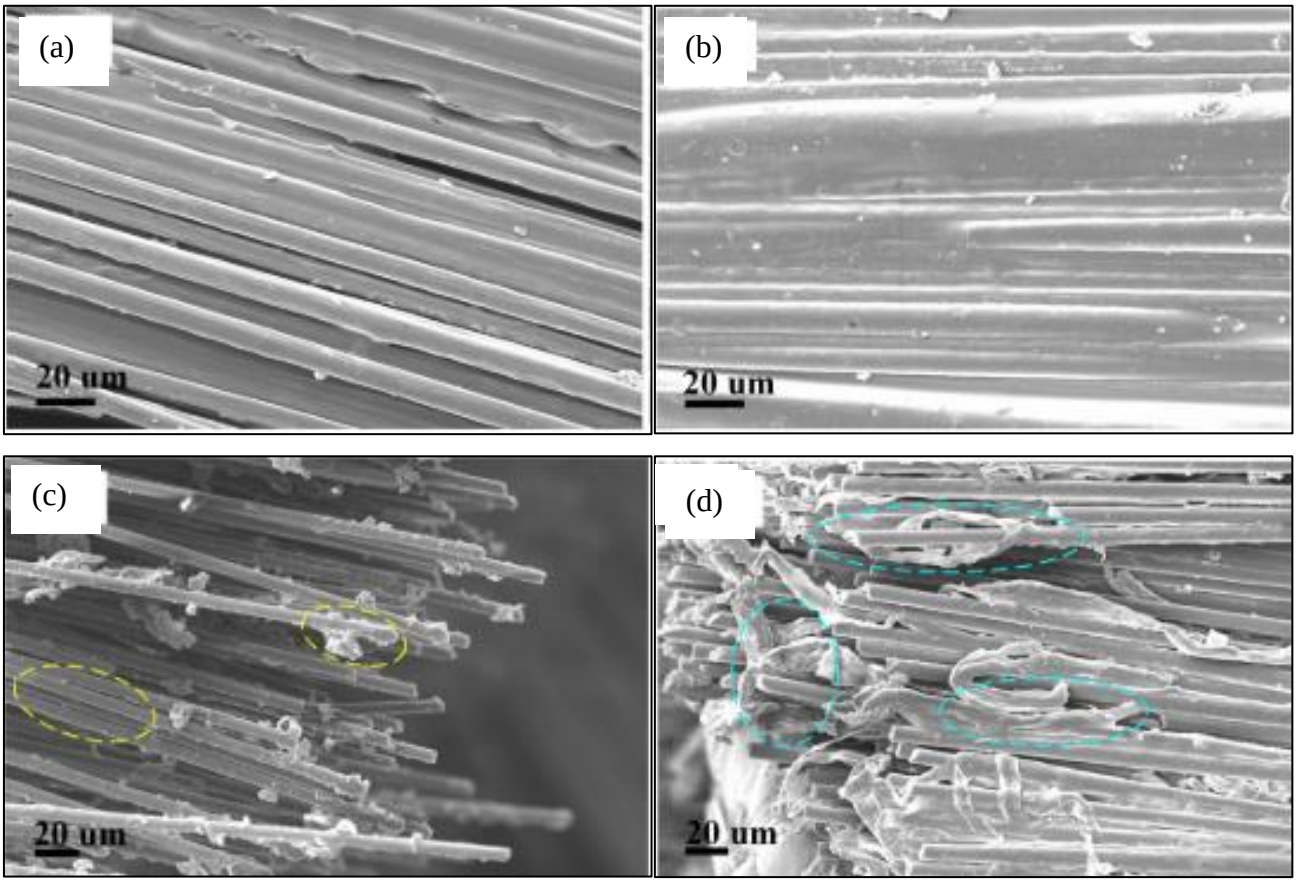


FIGURE 16. SEM micrographs of produced composites specimens of (a) non-modified CCFR-PLA (b) modified CCFR-PLA (c) fiber pull out of non-modified CCFR-PLA after tensile test (d) fiber pull out of modified CCFR-PLA after the tensile test (adapted from Li et al. 2016.)

### 3.2.3 Recycled wood fiber

Le Duigou et al. researched to understand the mechanical properties of wood fiber reinforced PLA. The different printing and compressing angles (90° and 0°) were tested to understand the effect of wood fiber distribution on tensile behavior and properties. Further, the printing width was adjusted (0.3, 0.6, 0.9 mm) and the sample properties were studied. (Le Duigou et al. 2016.) Further process information is described in Table 13.

TABLE 13. Process information of PLA reinforced with recycled wood fiber (adapted from Le Duigou et al. 2016.)

| | |
|---|---|
| **Parameter** | Method of printing: CM, FDM<br>Compressing angle: 0°, 90°<br>Printing angle: 0°, 90°<br>Width of the sample: 100 % 0.367 mm [0.3 mm], 200 % 0.557 mm [0.6 mm], 300 % 0.823 mm [0.9 mm] |
| **Material** | Woodfill fine filament: a blend of PLA and PHA reinforced with recycled wood fibers: Wood fiber ≈15.2 wt.% (range of 10~20 wt.%), diameter: 2.85 mm |
| **Process equipment** | 3D printer (Prusa i3 Rework, maximum printing area: 19×19cm$^2$)<br>software (Repetier host v1.0.6×Slic3r slicer) |
| **Experiment process** | Ready processed filament material is supplied<br>Test specimen production:<br>Tensile, actuation test specimen dimension: L: 70 mm, W:10 mm<br>Accurate test specimen dimension: 1000 cm$^3$<br>Printing angle: 0°, 90° |
| **Nozzle temperature in °C** | 210 |
| **Bed temperature in °C** | 70 |
| **Layer height in mm** | 3 |
| **Nozzle diameter in mm** | 0.4 |
| **Printing speed in mm/s** | 18 |

The orientation of the wood fiber in the samples were assumed to be brought by the extrusion process of filament production as the tensile properties of the 0° printed samples were very similar with the CM samples. Further, CM samples showed lower void content than FDM samples as CM method applies much higher pressure to the samples leading to better adhesion of layers. With increase of printing width, the melting and the blending pressure of the printing beads tend to decrease resulting lower layer adhesion and more formation of voids. Further, higher porosity was shown in order of 0°, 90°, and CM. The 0° printed samples showed higher porosity by 14.7, 15.5, and 21.8 % to CM and by 8.4, 11.1, and 14 % to 90° printed samples with printing widths of 0.3, 0.6, and 0.9 mm. With increase of printing width, the extrude throughput volume increased and lowered the extrude nozzle pass. This showed a negative effect on the adhesion between layers and lowered the mechanical behavior and ductility. The lower porosity in 90° was assumed from better packing between melt extrudes which were resulted from a faster pass of melts, derived from the geometry shape. Also, higher tensile strength and tensile modulus were shown in order of CM, 0°, and 90° printed samples. Due to the circumstances of using a natural fiber as composite, the water uptake rate was measured. Wood as a natural fiber tends to have a high water uptake rate, tending to swell the produced samples. In addition, with a higher value of the width, the water uptake rate increased. (Le Duigou et al. 2016.)

### 3.3 Composite based on polypropylene (PP) and polyethylene (PE)

In this sub-chapter, recent development of composite based on PP and PE are collected. The process methods and parameters are tabulated and their effect are described in the text.

#### 3.3.1 Glass fiber/ maleic anhydride polyolefin

Sodeifian et al. experimented to reinforce the PP matrix with the addition of GF and maleic anhydride polyolefin (POE-g-MA). The objective of the research was to study the mechanical and morphological properties at different infill of POE-g-MA, different layer height, and the presence of GF. (Sodeifian et al. 2019.) More process information can be seen in Table 14.

TABLE 14. Process information of PP reinforced with GF and maleic anhydride polyolefins (adapted from Sodeifian et al. 2019.)

| | |
|---|---|
| **Parameter** | Infill of Maleic anhydride polyolefin (POE-g-MA): 10, 20, 30 wt.%<br>Layer height : 0.1, 0.4 mm<br>Addition of GF |
| **Material** | PP (H1500)<br>PP with 30 wt.% GF (density 1.16 g/cm$^3$, MFI 230 ℃/2.16 kg, shrinkage factor > 0.2 %)<br>POE-g-MA (density 0.9 g/cm, MFI 190 ℃/2.16 kg, softening point 90 ℃) |
| **Process equipment** | Single-screw extruder (Haake, L/D 26), FDM 3D printer (SIZAN$^2$), CM machine (WCH) |
| **Experiment process** | Filament production:<br>Different infills of PP, PP-GF30 wt.%, and POE-g-MA were mixed and extruded to a filament with a single-screw extruder in a different range of process temperature (175-200 ℃). Filament diameter: PP: 1.7 mm, reinforced PP: 1.45-1.59 mm<br>Test specimen production:<br>Tested in CM and FDM printing<br>FDM: dimension: ASTM D638-V<br>Printing direction: not mentioned, a triangular filling pattern<br>CM: filaments converted to granules and mixed in the extruder<br>Mixed granulate formed into sheets (preheated: 200 ℃ at 5 MPa 6 min then 50 MPa for 1 min, machine off and let cool down to atmosphere) ASTM D638-V shape by a punch tool |
| **Nozzle temperature in °C** | 240 |
| **Bed temperature in °C** | 30 |
| **Layer height in mm** | 0.1, 0.4 |
| **Infill density in %** | 100 |

GF reinforced PP specimen resulted in higher tensile strength (≈34 MPa) and modulus (≈400 Pa) compared to the pure PP specimen (≈20 MPa, ≈55 Pa). However, showed lower flexibility and elongation at break (PP:≈24.3 %, PP-GF:≈8.3 %) as the GF restricted the polymeric chain movement. To redeem the decreased flexibility of GF reinforced PP an elastomer modifier, maleic anhydride polyolefin (POE-g-MA), was added by different weight percentages of 10, 20, 30 wt.%. The SEM analysis of POE-g-MA added samples showed accumulation of polyolefin around the GF surface which was resulted from the reaction between the MA group of the POE-g-MA and the hydroxyl group of the GF surface. The reaction increased with increase of polyolefin content (from POE-g-MA) which brought improved stiffness to the structure. Another factor shown in the samples was POE-g-MA tending to be isolated from the surface of the GF and PP matrix leading to phase separation and formation. These factors resulted in larger elongation at break, higher flexibility, however a decrease in strength. As the weight percentage of POE-g-MA increased these impacts were emphasized. Specimen were produced by two methods of FDM printing and CM. The CM specimen showed higher tensile strength at PP-GF (CM:≈ 42 MPa, FDM:≈ 34 MPa), PP-GF-10 wt.% POE-g-MA (CM:≈ 34 MPa, FDM:≈ 34 MPa) and PP-GF-30 wt.% POE-g-MA (CM:≈ 25 MPa, FDM:≈ 20 MPa). However, in the same material mixtures, FDM specimens showed higher elongation at break point (PP-GF: CM≈9 %, FDM≈8.5%, PP-GF-10 wt.% POE-g-MA: CM≈9 %, FDM≈11 %, PP-GF-30 wt.% POE-g-MA: CM≈9.1 %, FDM≈7.2 %) leading to better flexibility. The material mixture of PP-GF-20 wt.% showed a different mechanical characteristic. It showed superior tensile strength (CM: 24 MPa, FDM: 26 MPa) and flexibility (CM: 8.5 %, FDM: 11 %) with FDM than CM. To understand the effect of layer height on the specimen, layer heights of 0.1 and 0.4 mm were tested. Samples with 0.1 mm resulted in higher tensile strength. Sodeifian et al. claimed that it was due to the enhance of inter-layer adhesion with lower layer height. (Sodeifian et al. 2019.) This claim was supported by other reports (Onwubolu and Rayegani 2014, Li, Wang, Sun & Yu 2018, Sharma, Singh, Penna & Fraternali 2018).

### 3.3.2 Microsphere

Wang et al. experimented to understand the mechanical properties of PE-based polywax matrix reinforced with microspheres. Microspheres are thermally expandable to 50-100 times of its initial volume in a heated environment. Hence, microspheres can reduce the voids between layers enhancing mechanical properties. These microspheres must be treated below 120 ℃ to prohibit expansion during the FDM extrusion. Therefore PE, a polymer with a low melting point was used in this experiment. The parameters were set with different microsphere weight percentage, sample thermal treatment

temperature, and heating time. (Wang et al. 2016.) Additional process information can be seen in Table 15.

TABLE 15. Process information of PE-based polywax reinforced with microsphere (adapted from Wang et al. 2016.)

| | |
|---|---|
| **Parameter** | Infill of Microsphere: (0, 2, 5, 8, 11 wt.%)<br>Thermal treatment: 130-180 ℃ / 10 ℃ interval<br>Printing time: 40-120 s/ 20 s interval |
| **Material** | Microspheres (Expancel 930DU120, Initial foaming T: 120 ℃)<br>PE-based polywax (melting T: 95 ℃, Melt flow index: 19 g/10 min, linear heat shrinkage) |
| **Process equipment** | Twin screw-extruder (HAAKE), single-screw extruder, FDM machine (HY3D Corporation) |
| **Experiment process** | Compounding:<br>Microspheres and polywax mixed for 10 min and compounded in twin screw extruder for masterbatch of microspheres 20 wt.%<br>Filament production:<br>Masterbatch and polywax mixed and extruded in single-screw extruder producing filament (diameter: 2.5 mm)<br>Test specimen production:<br>Specimen dimension: ISO 527 5A dog-bone, ISO 604 pipe cylinder<br>Printing direction: not exactly mentioned<br>Postprocess of test specimen:<br>Test specimen thermal treatment between press plates with a distance of 15 mm which has a silk net between<br>Thermal treatment: 130-180 ℃ / 10 ℃ interval<br>Time: 40-120 s/ 20 s interval |
| **Nozzle temperature in °C** | 100 |
| **Printer bed temperature in °C** | Atmosphere temperature |
| **Nozzle diameter in mm** | 0.5 |
| **Layer height in mm** | 0.2 |
| **Printing speed in mm/s** | First layer: 30, other layers: 50 |

Higher microsphere content resulted in a decrease of porosity. This reduced die swells and enhanced better adhesion between deposition lines. As a result, tensile strength (0 wt.%: range of 2.2- 2.8 MPa, 11 wt.%: range of 3.7-3.9 MPa), compressive strength, overall stiffness, and storage modulus increased. Microsphere content over 8 wt.% didn't result in a massive increase of compressive strength (8 wt.%: range of 5.1- 6.3 MPa, 11 wt.%: a range of 5.1- 6 MPa) but showed similar results as microsphere agglomeration were caused resulting stress concentration and accumulation of inter-particle voids. The decrease of void content and the increase of microsphere agglomeration by increase of microsphere infill can be seen in Figure 17. The increase of thermal treatment temperature increased tensile strength and

compressive strength for neat PE specimens. Specimens of 2 wt.% microsphere reinforced composite also showed improvement till an optimum value (tensile: ≈ 2.65 MPa, compressive: ≈ 3.1 MPa) at around 140 to 150 ℃ however, a decreased afterward. This was due to the expansion of microspheres at 180 ℃, producing stress concentration propagating cracks along with the microspheres and layers. The treatment heating time effects differed with the loading of microspheres. With increase of heating time, low loading showed a positive effect, however with the loading of 8 wt.% or more the increase was less significant. (Wang et al. 2016.)

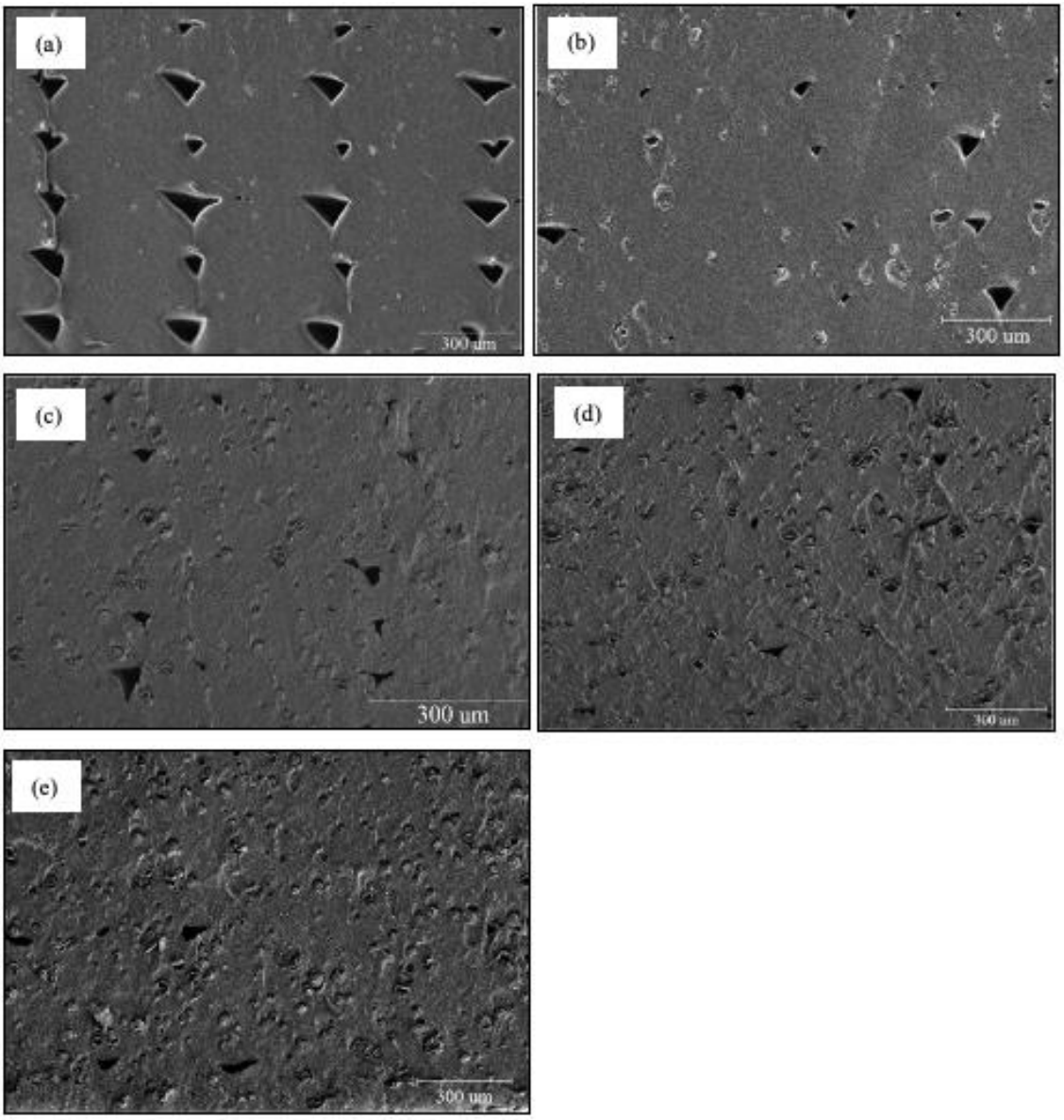


FIGURE 17. SEM micrograph of sample fracture processed at 140 ℃ (a) 0, (b) 2, (c) 5, (d) 8, (e) 11 wt.% (adapted from Wang et al. 2016.)

# 4 RECENT DEVELOPMENTS IN LARGE SCALE DIRECT PELLET EXTRUSION METHOD

Recent years studies of applying AM in large-scale structures has increased due to its benefits of rapid and automated production, reduction of process steps, high freedom of design, and possibility of optimization (3d-printers, Marrett 2018, Love, Kunc, Rios, Duty, Elliott, Post, Smith & Blue 2014; Wu et al. 2016; Boyd, Weller, Disanto, Rees & Hilbert 2017; Duty et al. 2017; Biswas, Rose, Eikevik, Guerguis, Enquist, Lee, Love, Green & Jackson 2017; Liu, Chi, Jiao, Tan, Liu & Yang 2017; Compton et al. 2017; Delgado Camacho, Clayton, O'Brien, Seepersad, Juenger, Ferron & Salamone 2018).

The scale-up process provides a possibility for AM applications in industries such as building and construction, boat construction, and sporting goods (Gibson et al. 2015, 9). For producing large-scale structures, materials in form of direct pellets are preferably used instead of processed filaments due to its advantages of cost reduction, acceleration of production, and widely available materials (Liu et al. 2017). Therefore, numerous investigations on direct-pellet extrusion are rising. However, factors adversely affecting the mechanical properties such as residual stress, warping, and voids are increased when producing larger-scale structures. Further, small thermal rate changes on the basic build structure significantly affect the residual and internal stress. (Compton et al. 2017.) Moreover, large-scale components manufactured with thermoplastic result in low stiffness and strength at the presence of load. (Wu et al. 2016, [Paolini, Kollmannsberger, and Rank 2019, 5]). To overcome these effect, research on large-scale direct pellet extrusion modification are rising such as reinforcing polymer materials, optimizing process parameters, and adding extra process methods. (3d-printers; Biswas et al. 2017; Boyd et al. 2017; Compton et al. 2017; Delgado Camacho et al. 2018; Duty et al. 2017; Liu et al. 2017; Love et al. 2014; Marrett 2018; P. Wu et al. 2016.)

The commercialized and developed technology of large-scale direct pellet extrusions is categorized by its process method in Table 16. The process method is mainly divided into gantry and robotic. The gantry system is based on the Cartesian coordinate system where the printing head moves in three axes of x, y, and z. The robotic system functions with a printing nozzle being located in a six-axis or more motion robotic arm. Gantry system is commonly used in small-scale AM applications therefore it is fairly easy to enlarge the size for large-scale applications however it has a limitation of one deposit direction (orthogonal), fixed size of the system, complication of transportation, and labor-intensive installation. The robotic system has a flexible process condition, requires less process space, and could

be easily transportable. Process methods that cannot be included in gantry or robotic will be categorized as others and it will be described afterward. (Delgado Camacho et al. 2018.)

TABLE 16. Example of material extrusion process in the construction industry using a polymer as the material (adapted from Delgado Camacho et al. 2018.)

| **Process method** | **Gantry** | **Robotic** | **Other** |
|---|---|---|---|
| Movement of printing head | Three axes | Over six axes | - |
| Process information | • One deposit direction (orthogonal to the printing bed)<br>• Require a larger system size than built component<br>• Complication of transportation<br>• Labor-intensive installation | • Flexible process condition<br>• Less process space required<br>• Easily transportable | - |
| Technology | BAAM<br>Qingdao Unique technology<br>KamerMaker<br>Large-scale double-stage-screw direct pellet extruder<br>LSAM<br>THE BOX | C-Fab | Mini-Builders |

In this chapter, research articles and commercialized products on large-scale direct pellet extrusion processes are collected. In research articles, processing parameters and raw materials are tabulated and described. In commercialized products, depending on the availability of the information, technical information are tabulated and described in the text. Furthermore, the limitation of the developed method and the possible improvements mentioned in articles are explained.

## 4.1 Gantry system

In this sub-chapter, the gantry process method technologies listed in Table 16 are collected. As mentioned before, for collected literatures, the process parameters and raw materials are tabulated and described. For collected commercialized products, depending on the availability of the information, technical information are tabulated and explained in the text.

### 4.1.1 Big Area Additive Manufacturing (BAAM)

The Oak Ridge National Laboratory (ORNL) has developed a large-scale material extrusion AM technique called Big Area Additive Manufacturing (BAAM). The build platform is capable of processing structure up to a length of 6 m, width of 2.4 m, and height of 1.8 m which is up to ten times larger than commercialized systems. The BAAM system is similar to FDM technology by extruding thermoplastic materials through a heated nozzle along specific tool paths to a heated build platform. It can process all thermoplastic material possible of injection molding or conventional fashion extrusion. However, BAAM system melts pelletized feedstock with a single-screw extruder and FDM melts a thin filament feedstock. With the pellet-based manner, the depositing rate could be 200 times faster and the feedstock costs could be 20 times reduced than a standard AM system which has polymer filament as material. (Duty et al. 2017.)

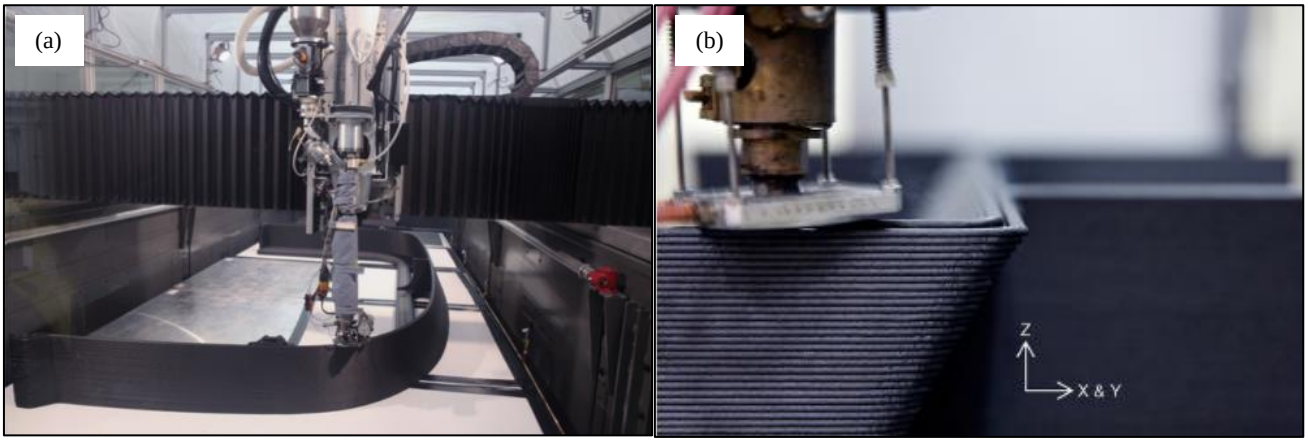


FIGURE 18. (a) BAAM system printing an Additive Manufacturing Integrated Energy (AMIE) section (b) close view of the layering process of BAAM (adapted from Biswas et al. 2017.)

The extrusion nozzle in the BAAM system is located orthogonal (z-axis) to the build platform and moves along the horizontal plane (x-y axis). The melted material exits the extruder through a circular orifice and contacts the heated build platform or the previously deposited layer. The material deposits as an oval shape with a width and height of 8.4 mm and 4 mm when using a 7.6 mm nozzle. The deposited bead shape and final product quality are dependent on material and process parameters such as extrusion temperature, printing bed temperature, print spacing, flow rate, head speed, and material property. Different parameter values are tested on BAAM technology to improve the quality of the product. (Duty et al. 2017.) The process conditions of BAAM could be seen in Table 17 and in Figure 18 the BAAM system producing Additive Manufacturing Integrated Energy (AMIE) project can be seen which will be explained later.

TABLE 17. Process condition of BAAM (adapted from Duty et al. 2017.)

| | |
|---|---|
| **Commercial product** | BAAM-CI by Cincinnati Inc. |
| **Maximum deposition rate in kg/h** | 50 |
| **Maximum build platform in $m^3$** | 6·2.4·1.8 |
| **Typical build platform temperature in ℃** | 95 |
| **Maximum operating temperature in ℃** | 365 |
| **Capable weight percentage of short fiber-reinforced material (<3 mm) in wt.%** | 40 |
| **Head/nozzle deposition orientation** | Located orthogonal to a horizontal build platform (z-axis)<br>Moves in parallel to the build platform (x-y axis)<br>material deposits vertical to the build platform (z-axis) |
| **Orifice nozzle diameter in mm** | 2.5-7.6 |
| **Deposited bead geometry in mm** | Oval shape<br>Nozzle 7.6 = Width: 8.4, Height: 4 |

Thermoplastic materials commonly used in the material extrusion process has a high thermal expansion coefficient up to 80-100·$10^{-6}$ m/mk (meter per meter Kelvin) leading vulnerability to warp and residual stress between layers. Compton et al. mentioned, these problems significantly increase during large-scale production and therefore conducted a simulation for analyzing the thermal evolution. Thin walls of CF reinforced ABS were fabricated via BAAM and its thermal evaluation was measured using infrared image and a simple 1D (one dimension) transient thermal model was designed to run simulations of the build process. The process information can be seen in Table 18. The layer temperature profile directly before depositing a new layer referred to the steady-state top layer temperature ($T_{top}$), was used as an indicator for the degree of warping and cracking as it most greatly influences the strength of the inter-layer bond, affecting the structural integrity of the build. (Compton et al. 2017.)

TABLE 18. Process information of BAAM experiment conducted by Compton et al (adapted from Compton et al. 2017.)

| | |
|---|---|
| **Parameter** | Layering time: 39, 120, 300 s<br>Orifice diameter: 5.1, 7.6 mm<br>Wall height: 5, 11, 20, 40 mm<br>Ambient temperature: 18, 40, 60, 80, 100 ℃<br>Deposition temperature: 180-230 ℃<br>Bed temperature: 20, 65, 100, 140 ℃<br>Thermal conductivity on (k) |
| **Material** | ABS with 20 wt.% CF (Techmer Electrafil J-1200/CF/20), density: 1140 kg/m$^3$ |
| **Process condition** | Build volume 3.56·1.65·0.86 m$^3$<br>Walls volume: 1.542·0.02·0.358 m$^3$<br>Process consist of gantry system (constant velocity 101.6 mm/s), Single screw extruder (diameter 25 mm), heated bed |
| **Experiment process** | <u>Pellet preparation:</u><br>Feed pellets (diameter 3 mm length 3mm) dried at 60 ℃ for minimum 4 h<br><u>Test specimen production:</u><br>The first layer is deposited on an ABS sheet which is heated on an Aluminum bed at 90 ℃<br>The top layer of ABS sheet maintains a temperature of 65 ℃<br>Vacuum used to maintain the level surface of sheet during printing<br>Sheet is separated from the heaters by a thin wire mesh<br>Extruder configured with orifice of diameter of 7.6 mm or 5.1 mm<br>Molten polymer exits the extruder of<br>Height: 3.8 mm width: 8.6 mm (7.6 mm orifice)<br>Height: 2.54 mm Width: 5.5 mm (5.1 mm orifice) |
| **Nozzle temperature in** ℃<br>**Orifice exit temperature** | 180-230 |
| **Printer table temperature in** ℃ | 20, 65, 100, 140 |
| **Layer height in mm** | 4.064 |
| **Nozzle diameter in mm** | 25 |

The experiments resulted in rapid cracking and delamination of substrate when $T_{top}$ dropped under the glass transition temperature ($T_g$). Therefore, during the experiments of different parameters, the developed $T_{top}$ value was compared to the $T_g$. Compton et al. concluded an aligned order of parameters which influences most to a successful printing: wall thickness > ambient temperature > deposition temperature > bed temperature. Increase of wall thickness led to decrease of surface-to-volume ratio and increase of layering time. This led to lower layer surface area rate and heat loss rate of $T_{top}$ which resulted in less warping and cracking of deposit layers. Increase of ambient temperature resulted in

slower heat loss of $T_{top}$ which decreased the rapid cracking and warping. The deposition temperature and bed temperature did not have much influence on the $T_{top}$ value. On the other hand, the material properties and deposition parameter experiments derived that increasing the thermal conductivity of the feedstock had a negative effect on successful printing with large-scale objects. (Compton et al. 2017.)

Biswas et al. cooperated in a research project Additive Manufacturing Integrated Energy (AMIE) to manufacture a cylindrical-like architect structure with BAAM shown in Figure 19. AMIE aimed to construct building towards an energy-efficient approach, with less material, less waste, and less energy during operation. The segments were printed as a half-ring structure and assembled producing 19.5 $m^2$ ground area and 2.8 m height. (Biswas et al. 2017.) Brief process information can be seen in Table 19.

TABLE 19. Process information of cylindrical-like architect structure (adapted from Biswas et al. 2017.)

| **Parameter** | Printing angle |
|---|---|
| **Material** | CF reinforced ABS |
| **Process information** | Ground area: 19.5 $m^2$ height: 2.8 m<br>6136 kg ABS material<br>225 h building time |

The rounded and curved surfaces reduced localized stresses. The building design attempted to overcome two limitations of the BAAM system: the structural weakness when printing in the z-axis and the maximum cantilever angle for depositing layers of the printed material. The whole length of the building was followed by steel rods to post-tension the structure resulted from lack of strength by z-axis printing. The cantilever angle of exterior rings was kept below 40° from the horizontal to reduce insufficient contact between the printing layers and prevent sag of printed material. In result, the low tensile strength and stiffness issue of carbon-reinforced build structure was resolved. (Biswas et al. 2017.)

FIGURE 19. Cylindrical-like architect structure printed by BAAM (adapted from Biswas et al. 2017.)

Duty et al. researched to investigate the deposited structure and mechanical properties of the printed materials derived by the BAAM in the initial development stage. During the experiment, the stiffness, tensile strength, and tensile modulus were measured. (Duty et al. 2017.) The process of information can be seen in Table 20.

TABLE 20. Process information of the BAAM experiment conducted by Duty et al (adapted from Duty et al. 2017.)

| | |
|---|---|
| **Parameter** | Printing axis: x, y, z<br>Matrix: ABS, PPS, PEI<br>Composite fiber: CF, GF, CFTF wt.%<br>Printing speed: high speed: 16 kg/h<br>Orifice size: small orifice (sm)= 5 mm, normal= 7.6 mm<br>Deposition temperature: 207 ℃, 250 ℃<br>Screw design: retrofit screw, original Dohle extrusion screw<br>Addition of z-tamping |
| **Material** | ABS (SD-0150 W)<br>ABS/13%CF (AS-13CF/000 Black)<br>Techmer 5 MFI high impact ABS<br>Techmer HiFill J-1200/20 NAT<br>J-1200/CF/20, ABS (TES) – chopped carbon fiber CFTC<br>Techmer HiFill 1305-11007 NAT |
| **Process information** | Structured with gantry system, single-screw extruder, heated bed, Print angle: 90° |
| **Experiment process** | Test specimen production:<br>Single-screw extruder melts pelletized feedstock<br>Feedstock melts deposited through single extrusion screw with 7.6 mm extrusion orifice at a rate of 4.5 kg/h onto an unheated build platform<br>Dimension: ASTM D638 type 1<br>Printing direction:<br>x-axis= sample cutting that the primary load is parallel to the deposition direction<br>y, z-axis= sample cutting that the primary load were orthogonal (horizontal, vertical) to the bead axis<br>Post-process of test specimen:<br>Samples dried at 50 ℃ for at least 48 h and held in a desiccant chamber at 23 ℃ for at least 15 h |
| **Nozzle temperature in ℃ ABS/ABS-13%CF** | 207/250 |
| **Printer table temperature in ℃** | 65 |
| **Layer height maximum in mm** | 4 |
| **Nozzle diameter in mm** | 2.5-7.6 |

The neat ABS sample printed by BAAM showed low dependence on printing direction for tensile strength and stiffness with under 25 percent variation. Along, the stiffness of the neat ABS samples was comparably strong as the injection-molded samples. Carbon fiber reinforced samples (13 wt.% CF-ABS) showed significant improvement of stiffness and strength along the deposition direction and by addition of higher fiber content (20 wt.% CF-ABS) when printed with an original screw. However, the strength and stiffness tested at the direction of the z-axis (interlaminar) were rarely 40 percent more than at the x-axis (tool path) showing a high degree of anisotropy. This leads to BAAM products only possible for stiffness-limited applications. Fiber-reinforced samples showed a higher degree of inner and inter-void. To lower the void formation, the technique of *z-tamping* shown in Figure 20 was tested. In this technique, the extruder is located at the center of an air-cooled platen vibrating at around 20 Hz, flattening the layers. It pressures new deposited beads into nearby pores while the bead is still warm and in pliable conditions. This increased the flow of fiber-reinforced materials and improved interlayer adhesion. By z-tamping, the tensile strength of the test specimen of ABS-CF 13 wt.% increased approximately 114 % (≈ 53 to 59 MPa) when printing in the x-axis direction and approximately 192 % (≈ 13 to 25 MPa) in the y-axis direction compared to the non-z-tamping test specimen. Further, tensile modulus was increased by approximately 109 % (≈ 8.2 to 8.9 GPa) in the x-axis and 132 % (≈ 2.2 to 2.9 GPa) in y-axis. Even though the improvement of z-tamping at the y-axis was much higher, the x-axis has a generally higher tensile value, therefore brings better mechanical properties in the end. A variety of material tests were conducted by BAAM and showed the possibility to print composite materials with high strength over 60 MPa and stiffness up to 12 GPa. However, due to the high degree of anisotropy researchers are investigating to reduce its value and produce a consistent mechanical performance for needed applications. (Duty et al. 2017.)

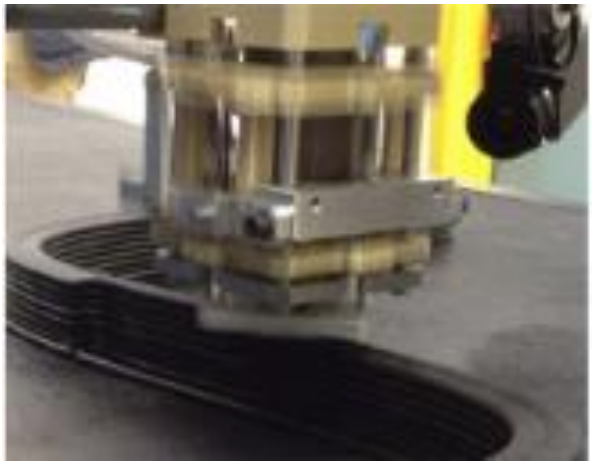

FIGURE 20. Process of z-tamping (adapted from Duty et al. 2017.)

### 4.1.2 Large-scale double-stage-screw direct pellet extruder

Liu et al. designed a large-scale double-stage-screw FDM 3D printer using plastic pellets as process material. (Liu et al. 2017.) Its structure is shown in Figure 21.

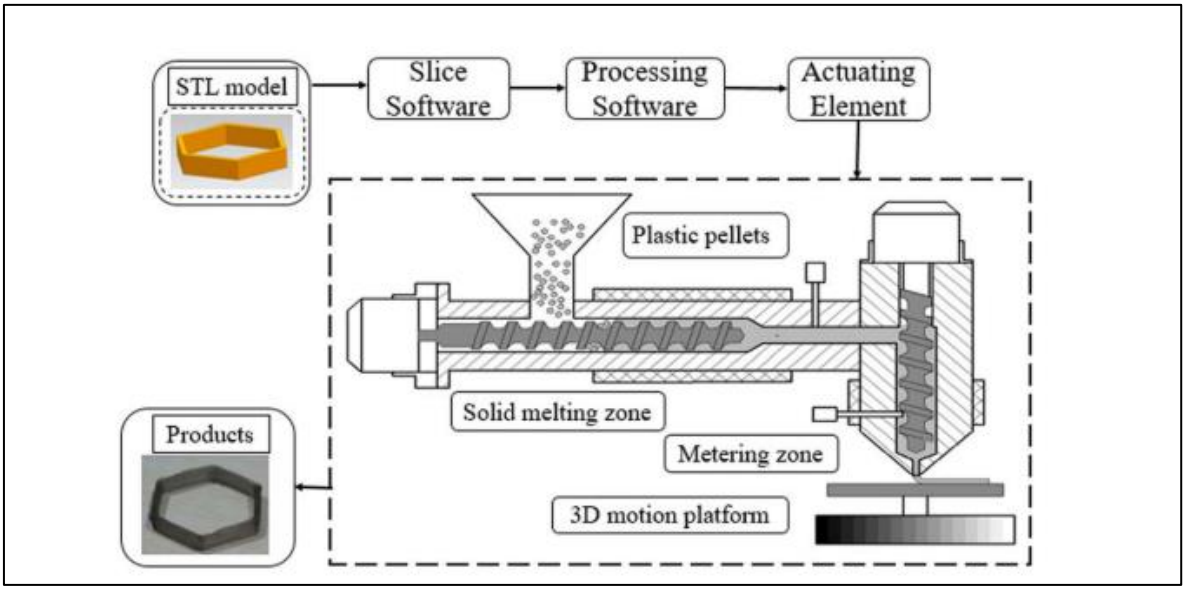


FIGURE 21. Structure of the large-scale double-stage-screw direct pellet extrusion (adapted from Liu et al. 2017.)

Various back pressures in the cylinder and different rotating speeds were tested to study the effects on the melt flow rate. An equation relating these three parameters were established and were used to investigate experiments on melt flow, printing speed, and layer height of the width. Also, effects of printing spacing on bonding strength and surface accuracy were analyzed. (Liu et al. 2017.) The process information can be seen in Table 21.

TABLE 21. Process information of Large-scale double-stage-screw direct pellet extruder. (adapted from Liu et al. 2017.)

| | | | |
|---|---|---|---|
| **Parameter** | Back pressure (P) (4, 5, 6, 7, 8, 9, 10 MPa)<br>Speed of metering screw (n)<br>(-18, -15, -12, -6, -3, 0, 3, 6, 9, 12, 15, 18 rpm)<br>Printing spacing (ε) (2, 2.5, 3, 3.5, 4 mm) | | |
| **Material** | ABS757-GF10 (GF 10 % mass fraction)<br>melt index: 3.8 g ·10 $min^{-1}$ (230 ℃), density = 1.26 g ·10 $cm^3$<br>thermal expansion rate 0.33 % | | |
| **Process equipment** | Build platform: 800·600·600 $mm^3$<br>Model 1 (casting mold):<br>180·100·50 $mm^3$ (machine allowances: 5 mm)<br>P= 7 MPa, n= 8 rpm, extruding speed ($v_r$)= -30 rpm, printing speed (v)= 20 mm/s, layer height (h)= 2.0 mm, ε= 2.5 mm heating temperature of cylinder ($T_c$)= 230 ℃, heating temperature of platform ($T_p$) = 80 ℃<br>Model 2 (printer):<br>650·650·800 $mm^3$<br>P= 7 MPa, n=13 rpm, $v_r$= -30 rpm, v=30 mm/s, h= 2 mm, ε= 3 mm, $T_c$ =230 ℃, $T_p$=80 ℃ | | |
| **Material process** | Pellets are dried 2 h in a vacuum oven at 90 ℃ before the printing process<br>Pellets are filled in a hopper.<br>Pellets pass the two-stage screw of diameter 25 mm and 16 mm.<br>Vertical milling machine: extrusion equipment fixed on Z-axis, platform move along Y and Z direction. | | |
| **Nozzle temperature in** ℃ | 230 | **Printer table temperature in** ℃ | 80 |
| **Layer height in mm** | 2.0 | **Nozzle internal diameter in mm** | 4 |
| **Printing spacing in mm** | 2.5 | **Nozzle external diameter in mm** | 8 |
| **Fused diameter in mm** | | | 3.2-3.3 |

The flow rate of the extrude increased linearly to the increase of backpressure (back pressure in MPa, melt flow in g/min: approx. 4, 1.78/ 5, 2,4/ 6.2, 2.9/ 7.1, 3.3/ 8.2, 3.7/ 9.3, 4.7/ 10.1, 5.7). The outcome showed the width of the fused filament increased as the melt flow increased and decreased as the layer height and printing speed decreased. For strong bonding strength, enough bonding area should be created between the filaments with avoidance of overflow and overlapping of the fused layers. Therefore, the width of the fused filament should be in between the internal and external diameter of the nozzle. The reduction of printing spacing increased the internal filling rate and the height of the model followed with an improved surface accuracy. In addition, reduction of printing spacing increased tensile strength and tensile modulus. However, as the printing spacing decreased to 2 mm, the surface quality decreased due to the overflow of unwanted accumulation. Printing spacing larger than the width of deposited filament produces no bonding strength between the filaments as there is no connection. In Figure 22, the

longitudinal view of tensile specimens deposited in different printing spacings can be seen. The printer optimization was done to successfully print the samples however, the unstable melt flow and the flow control were not able to be controlled. In conclusion, Liu et al. suggested adding a pressure stabilized extruder and an extruding system that can control melt flow precisely. (Liu et al. 2017.)

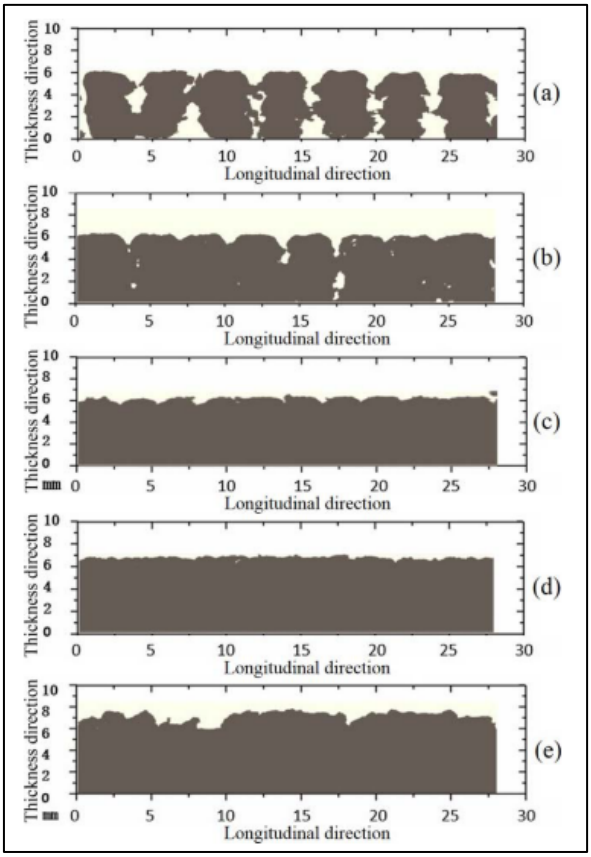


FIGURE 22. Longitudinal direction view of deposited layer depending on different printing spacing in order of (a-e) printing spacing of 4, 3.5, 3, 2.5, 2 mm (adapted from Liu et al. 2017.)

### 4.1.3 KamerMaker by Amsterdam-based architects

Amsterdam-based DUS Architects have developed a 3D printer, KamerMaker which has a capacity of fabricating dimensions of 2.2·2.2·3.5 $m^3$ with PP components (Wu et al. 2016 [Bogue 2013]). It was used in a 'Research & Design by Doing' project to fabricate a 3D canal house. (About the 3d print canal house n.d.) Here, materials of a bio-plastic mix containing 75 % plant oil and microfiber reinforced material were used (Wainwright 2014).

### 4.1.4 Large-scale fused deposition modeling printer by Qingdao unique technology

In 2014, Qingdao unique technology exhibited a large-scale FDM printer of size 12·12·12 $m^3$ with a one-step modeling process and shorter printing cycle. The printer deposits melt-material in a millimeter-level precision and use glass-reinforced polymer as printing material. This provided anti-corrosion, anti-aging, and waterproof functions. (Wu et al. 2016 [Feng and Yuhong 2014].)

### 4.1.5 THE BOX SMALL, MEDIUM, LARGE by BLB Industries AB

BLB industries AB commercialized three different large-scale 3D printers called THE BOX which can be seen in Figure 23 (3d-printers.n.d).

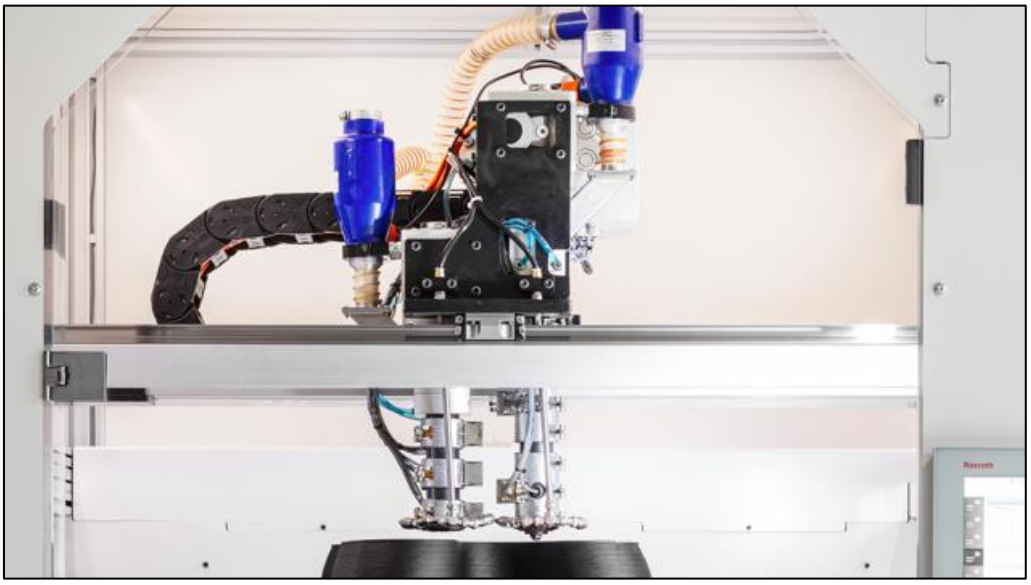

FIGURE 23. THE BOX LARGE of BLB Industries AB (adapted from 3d-printers n.d.)

The fabrication process is held in a vacuum environment which is made in a box, in addition, the deposition melts are extruded in a heated build plate. To control the cooling of the extruded parts, an option of a water cooling system can be added. (3d-printers n.d.) In Table 22, the technical specification of each product can be seen.

TABLE 22. Technical specifications of THE BOX SMALL, MEDIUM, LARGE from BLB Industries AB (adapted from 3d-printers n.d.)

| **Product** | **THE BOX SMALL** | **THE BOX MEDIUM** | **THE BOX LARGE** |
|---|---|---|---|
| **Build volume in mm$^3$** | 1500·1000·1000 | 1500·1500·1500 | 2000· 2000·1500 |
| **Maximum print speed in mm/s** | 600 | | |
| **Layer height in mm** | 0.5-4.0 | | 1.0-7.0 |
| **Maximum movement speed in mm/s** | 750 | | |
| **Nozzle size in mm** | 1.0-2.0 | 2.0-8.0 | 8.0-14.0 |
| **Maximum material output in kg/h** | 1.0 | 14.0 | 30.0 |
| **Number of extruders** | 2 | | |
| **Material options** | Standard Grade: ABS, PLA, Nylon<br>Special Grade: PP-glass fiber, PP-glass balls, ABS-wood fibers, ABS-carbon fibers, PE, PLA-wood fibers, PLA-copper powder, TPU, TPE | | |

### 4.1.6 Large Scale Additive Manufacturing (LSAM) by Thermwood

Thermwood manufacturers Large Scale Additive Manufacturing system (LSAM) machines functioning both 3D printing and trimming in the same machine. The LSAM works in a two-step and near-net-shape production process by first 3D printing the product in a slighter bigger size and trimming to its exact shape with a CNC router trimmer. The machine uses a “MELT CORE” print head which has tight control of print bead size, being able to change the bead dimension while printing and bring a good fusion between layers with void-free structures. The LSAM has a different approach instead of printing small beads in a heated environment, it prints large size beads at room temperature with a continuous cooling process and a compression wheel pressing the deposited round bead into a flattened bead fusing it with the previous layer. (Marrett 2018.) Detailed information of the LSAM models is shown in Table 23.

TABLE 23. Information on LSAM and LSAM MT (adapted from Marrett 2018.)

| **Model** | **Standard LSAM**<br>**Melt core: 40 mm** | **LSAM MT**<br>**Melt core: 60 mm** |
|---|---|---|
| **Material** | All thermoplastic | |
| **Capable printing size in $m^3$** | 3·1.5·1.5 or 3 | 3·1.5·5.1 or 12.2 |
| **Capable trimming size in $m^3$** | 3·1.8·1.5 or 3 | 3·1.8·5.1 or 12.2 |
| **Maximum output in kg/h** | 86.2-95.3 | 217.7-258.5 |
| **Maximum printable temperature in** ℃ | 450 | |
| **Printer table temperature** | Not heated (room temperature) | |
| **Material process** | Thermoplastic pellets are dried<br>Pneumatically conveyed to a vertically mounted print head<br>Print head melts thermoplastic material with heat<br>Melt-materials precisely meters through a heated print nozzle with continuous cooling controlled<br>Bead dimensions could be changed during the printing process<br>Bead compression wheel flatten the extruded bead and fuse it with previously deposited layer<br>Five-axis CNC router mounted on a separate print gantry trims the product | |

The pressing process of the compression wheel can be seen in Figure 24. This method led to print speed dependency on the cooling rate of the deposited polymer, rather than the nozzle output. Thus, each polymer is differently treated within its specific temperature range. (Marrett 2018.)

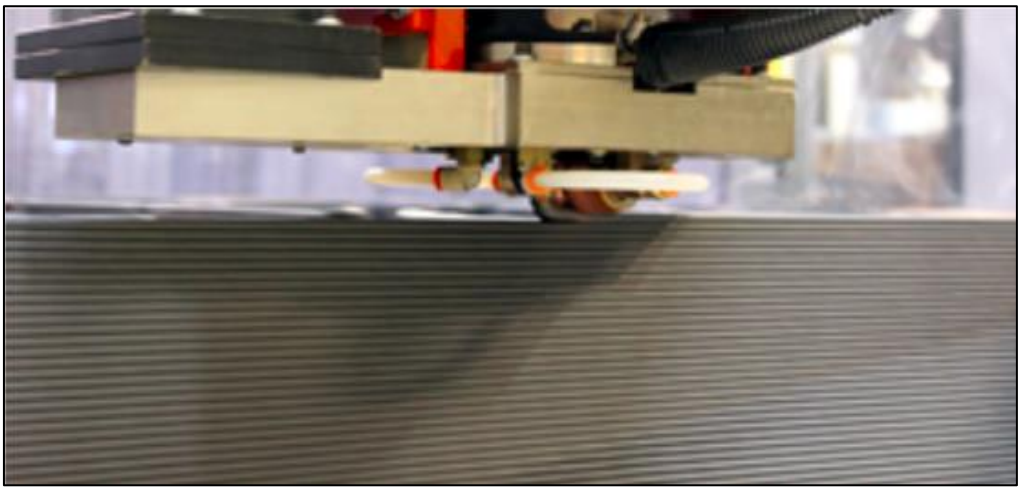

FIGURE 24. The deposited round bead being pressed by a compression wheel (adapted from Marrett 2018.)

## 4.2 Robotic system and other process method of large-scale direct pellet extrusion

In this sub-chapter, the robotic and other process method technologies listed in Table 16 are collected. As mentioned before, for the collected commercialized products, depending on the availability of the information, technical information are tabulated and explained in the text.

### 4.2.1 Cellular Fabrication (C-fab)

The company Branch Technology Inc developed a construction 3D printing technology called Cellular fabrication (C-FAB). This technology replicates the formation of a natural structure on a cellular level. In other words, plotting the deposition path based on a cellular structure and extruding the material by nozzle orifice shapes of Figure 25 which are based on natural formation shapes. C-FAB enables freeform fabrication and selective solidification of the extrudate in open space. Meaning, the extruder located in a robotic arm can deposit materials at any orientation and, the extrusion and cooling temperature can be controlled for needed solidification. In addition, adjustment of maximizing the extrudate surface area and minimizing the cross-section area can result in greater solidification. Any materials which can be extruded through an orifice and can rapidly solidify are used as a C-FAB material such as thermoplastic, thermoset, epoxies, metallic, foam, and ceramics. Reinforce fiber such as carbon or glass fibers are added to the matrix producing a composite of improved material properties (Heyman 2017). C-FAB fabricated structure provides extremely strong strength that is compatible with commercialized products. (Boyd et al. 2017.)

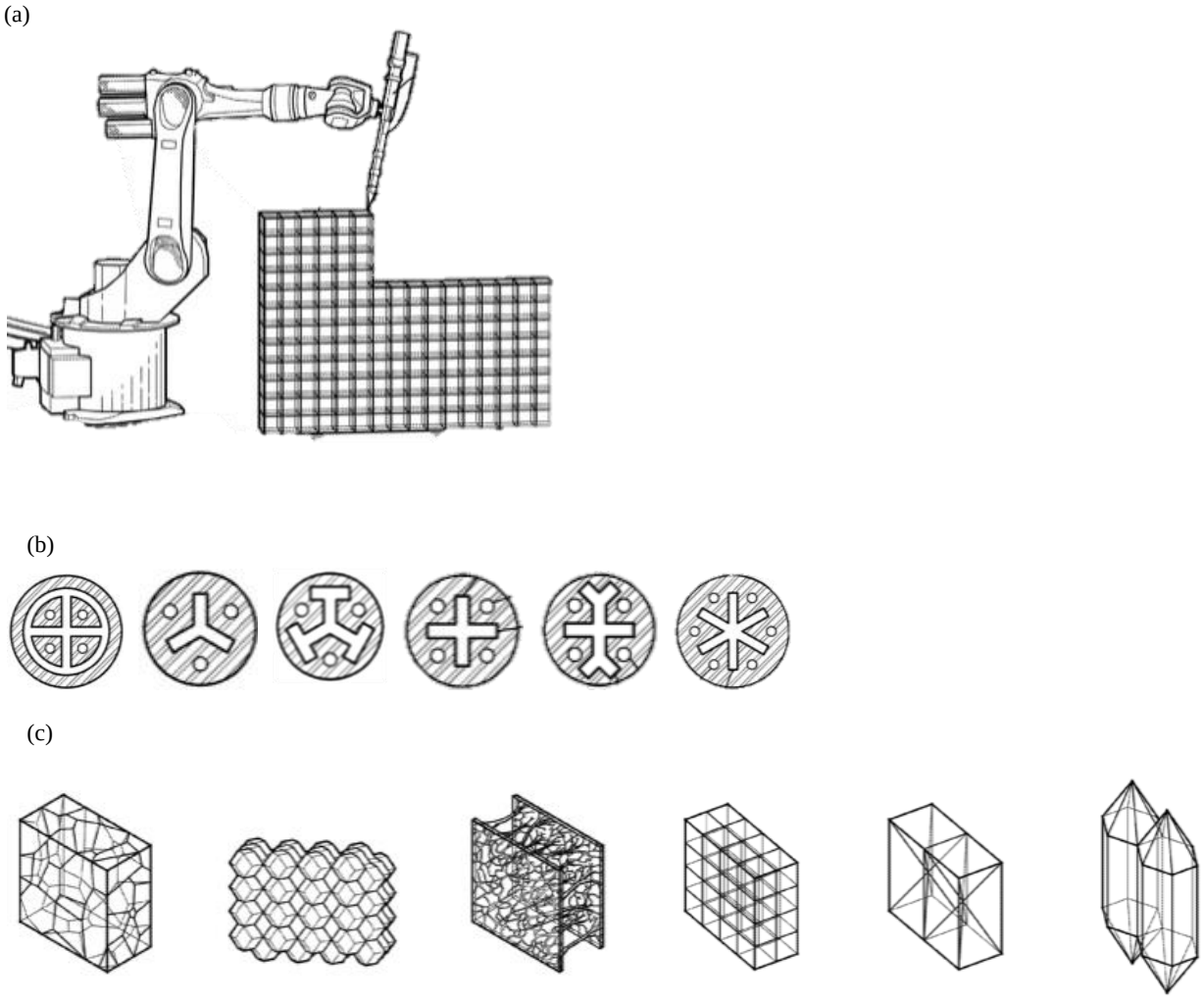


FIGURE 25. (a) Cellular fabrication (C-FAB) process schema, (b) nozzle shapes, (c) plotting's of deposition (adapted from Boyd et al. 2017.)

### 4.2.2 Minibuilders

Institute for Advance Architecture of Catalonia (IAAC) developed a 3D printing robot technology called Minibuilders. The Minibuilders consist of four robot machines which carry different functions of main, foundation, grip, and vacuum. The main unit robot is the brain of the Minibuilders operating the 3D printer. It is equipped with two material tanks, two-part polymer extruders, a connected robot movement controller, and wheels. The foundation robot fabricates the base in a precise pattern until the robot height limit (first 15 cm of the structure) is reached. Subsequently, the grip robot is attached to the foundation layers by four wheels, two on each side, and extrudes further structure parts. The nozzle can be dynamically moved sideways to allow curvatures along with the height of the object. Simultaneously to

the extrusion, heaters functions to fasten the speed of material curing time. The vacuum robot reinforces the printed structure by the other two robots. It attaches to the surface of the fabricated structure by a vacuum-operated suction cup and extrudes material nearly perpendicular to the structure layer by up and down movements. The deposition system is consisting of two parts which are located in different positions. One part is the nozzle located in each robot which receives material from two plastic hoses and blends it. The other part is a mechanical extruder located in the main robot which delivers the two components of material through the hoses to the nozzle. This extruder controls the deposition system and not each robot separately. The speed of the printer is relatively slow on the theoretical value of 0.03-0.05 $m^3$/h in the best case. The material used in the process is Axson Easymax which is consists of two component, polymer, and marble powder of ratio of 40 % to 60 %. (Jakupovic 2016; Jeffrey 2014.)

# 5 DISCUSSION AND INTERPRETATION

Throughout this part, the results from chapter 3 and 4 are summarized and discussed. The effect of reinforcing fiber/filler and each process parameters on mechanical properties of fabricated end products mentioned in literature are discussed. Further, the current developments and commercialized technologies mentioned in chapter 4 are summarized and reviewed.

## 5.1 Fused deposition modeling of polymer composites

Literature of recent developments on FDM of polymer composites were collected and reviewed. The review was focused on the scientific publications related to improving the mechanical properties of the FDM printed parts by reinforcing polymer materials and optimizing FDM process parameters. The reviewed reinforced polymers were ABS, PLA, PE and PP, and the reinforcing fillers and fibers were short/continuous/nano carbon fibers, glass fiber, jute fiber, wood fiber, iron metal powder, copper metal powder, and microsphere. The optimized process parameters were fill density, infill of reinforcing filler or fiber, printing temperature, printing angle, printing width, and printing layer height.

Depending on the reinforcing filler or fiber, the FDM printed parts resulted in an increase or decrease of tensile properties. Cu, Fe (Hwang et al. 2015), TPE, and jute fiber (Torrado et al. 2014) reinforced composite parts resulted in decrease of tensile strength and strain compared to pure polymer parts but an increase of Young's modulus. These reinforced composite printings showed inner-void formation which lead to lower layer adhesion. Further, the low degree of cross-linking molecules of elastomer structure tends to give a rubbery-like-elasticity property to the reinforced composite parts leading to higher flexibility and lower strength. Hwang et al. further studied the influence of Cu and Fe infill increase on the mechanical properties of printed parts. The increase of infill resulted in enlarged inner-void formation which further decreased the tensile strength. (Hwang et al. 2015; Torrado et al. 2014.)

Reinforced composite with filler or fiber such as CF (Tekinalp et al. 2014; Sezer and Eren 2019, Shofner et al. 2003; Li et al. 2016; Heidari-Rarani et al. 2019), GF (Sodeifian et al. 2019; Zhong et al. 2001), wood fiber (Le Duigou et al. 2016), $TiO_2$ (Torrado et al. 2014), graphene (Camargo et al. 2019) and microsphere (Wang et al. 2017) resulted in higher tensile strength compared with pure polymer printed parts. These composite parts showed a stepwise increase of tensile strength with higher filler or fiber

infill. However, from a certain point, the strength started to decrease or showed a plateau phenomenon. The exact reason was different from every literature but generally, it was due to the increase of fiber agglomeration, void formation around the fiber, and decrease in average fiber length which mainly occurred from FDM nozzle pass. These morphological properties resulted in lower adhesion of layers and stress concentration points which brought lower tensile strength. At the optimum value of tensile strength unfortunately the flexibility significantly decreased bringing brittleness to the structure. To redeem the flexibility, Zhong et al. (ABS-GF-LLDPE-hydrogenated Buna-N) and Sodeifian et al. (PP-GF-POE-g-MA) added a plasticizer (LLDPE, POE-g-MA). In both studies, the plasticizer positively affected the flexibility of the structure giving more movement to the polymer chains. However, it slightly lowered the tensile strength. In addition, with too much plasticizer, at one point the flexibility started to decrease. Zhong et al. researched further to redeem the lost flexibility and concluded the flexibility decrease was resulted by phase separation of the polymer matrix (ABS) and the plasticizer (LLDPE). The phase separation was reduced with the addition of compatibilizer (hydrogenated buna-N). The similarity of the chemical structures of the compatibilizer with the matrix and plasticizer resulted in prominent uniform dispersion leading to better mechanical properties and surface quality. (Camargo et al. 2019; Heidari-Rarani et al. 2019; Tekinalp et al. 2014; Torrado et al. 2014; Sezer and Eren 2019, Shofner et al. 2003; Sodeifian et al. 2019; Li et al. 2016; Le Duigou et al. 2016; Wang et al. 2017; Zhong et al. 2001.)

Le Duigou et al. (2016) claimed that fiber distribution of the printed parts is derived from raw filament fabrication as in the conducted experiment, the tensile properties of 0° printed and compressed samples were very similar when using the same filament. Further, literature of Tekinalp et al. (2014), Sezer and Eren (2019), Shofner et al. (2003), Zhong et al. (2001), Hwang et al. (2015), Torrado et al. (2014), Wang et al. (2017), Sodeifian et al. (2019) took this as a precondition by adding a material mixing process at the filament fabrication to achieve homogeneous fiber-polymer distribution at the FDM printed parts which resulted in lower fiber agglomeration and better mechanical properties.

The tested printing angles were mainly 0°, 90°, 45°, -45°. Depending on the study, the printing layers of the test specimen had uniform or two mixtures of printing angles, leading to various test specimen types. The reviewed literature in the thesis did not have enough overlapping test specimens which can be fairly compared therefore, the effect of the printing angle is generally analyzed. Test specimens containing a longitudinal printing angle, 0°, resulted in better tensile properties showing lower inner-void formation and higher-layer bonding compared to other printing angles. The experiment of Le Duigou et al. (2016) showed an exception by having higher tensile properties at 0° specimen even though having higher

porosity. Research of Shofner et al. (2003) also showed an exception by having higher mechanical properties at cross-layer alignment of 45° and -45°which resulted in the less inner-void formation and higher adhesion at the test specimen than at 0° and 90°. (Le Duigou et al. 2016; Sezer and Eren 2019; Shofner et al. 2003; Torrado Perez et al. 2014.) The direction of the tensile test is driven outward along the longitude of the test specimen. Hence, the 0° produced samples with a continuous extrusion path with the same longitude test direction could have resulted in better tensile properties.

The increase of printing width resulted in a higher extrusion volume flow rate and lower nozzle pass in the same sample geometry. This generally led to faster production time, however lower accuracy due to the difficulty of producing complicated dimensions with larger printing beads. Further, printing width increase decreased the melting and blending pressure of the print beads causing increase of void formation and lower layer adhesion. In result, the increase of the printing width of the layer brought lower mechanical properties. (Le Duigou et al. 2016.) Depending on the need for mechanical strength and accuracy of the end product, the printing width could be adjusted as it has a beneficial point of accelerating the production.

The effect of printing layer height on the mechanical properties of FDM end product was studied by Camargo et al. (2019) with materials of PLA and graphene reinforced PLA and Sodeifian et al. (2019) with PP and GF reinforced PP. Generally, the lower layer height showed improvement in inter-layer adhesion resulting in better tensile strength. This statement was also supported by other literature of Li et al. 2018, Onwubolu and Rayegani 2014, Sharma et al. 2018, Tymrak et al. 2014, and Chacón et al. 2017. However, the experiment of graphene reinforced PLA showed an exception by a significant increase of tensile and flexural strength with as increase of layer height (Camargo et al. 2019). This exception could be related with the structure of graphene which is one-layer of graphite. Unfortunately, Camargo et al. only concluded the results derived by changes of parameters but not the analyzation in a morphological or a chemical view.

Glass transition temperature and melting temperature of materials are different. Therefore, depending on the process materials the FDM printing temperature range varies. Hwang et al. (2015) researched to analyze the effect of printing temperature on the mechanical properties of FDM end parts. The increase of printing temperature resulted in a decrease of ABS material viscosity leading to a higher volumetric flow rate. These values influenced better adhesion between layers which brought better tensile strength and strain. Unfortunately, the effect of printing temperature on Cu and Fe filler reinforced ABS composites were not held nor discussed in the article. However, from the previously discussed factor, it

can be assumed that at the process parameter of higher printing temperatures, the ABS matrix with better flexibility could bond better with the metal reinforcements and result in improved mechanical properties.

CM is an efficient method that has a shorter process time than FDM. Therefore, literature have compared the mechanical properties of CM processed parts and FDM printed parts to analyze if the long printing time of FDM is profitable and necessary. The articles of Tekinalp et al. (2014), Le Duigou et al. (2016), and Sodeifian et al. (2019) resulted that CM parts have higher mechanical properties than FDM. Le Duigou et al. further compared the morphological properties of each CM and FDM parts and concluded the low tensile strength of FDM parts were derived by higher void formation during the printing process which led to low adhesion of layers. Sodeifian et al. (2019) further studied the effect of each process method on flexibility and reported that FDM parts have a higher percentage of elongation which indicates better flexibility. Also, at a certain amount of added elastomer modifier, the mechanical properties of FDM parts were slightly increased compared to CM specimens. This gave an insight that the CM method mostly brings better tensile properties and FDM process with better flexibility. There could be a good mixture point of FDM process to bring both better tensile strength and flexibility however, it shall be compared with the processing time and preparation needed for each method to find out which method is more profitable in the industry.

### 5.2 Large-scale direct pellet extrusion

The current state of commercialized large-scale direct pellet extrusion products and literature on improving the mechanical properties of large-scale direct pellet extrusion end products were reviewed. The reviewed large-scale direct pellet extrusion technologies were mainly categorized by the process method of the gantry and robotic. Gantry system has high feasibility leading to numerous developments and the robotic system has process flexibility bringing high potential developments. Except for the few differences in the production size, state of the feedstock, and the input method of feedstock, the large-scale direct pellet extrusion technology gantry system is very similar to the FDM technology. The influence of process parameter on the mechanical properties was similar too. Polymer composite structures result in improved tensile strength and stiffness compared to neat polymer structures and with an increase of filler or fiber infill, inner-void formation raised. (Duty et al. 2017.) However, large-scale production showed more radical effects with parameter changes resulting in higher void formation, warping, shrinkage, and residual stress which led to lower mechanical properties of the end product. Therefore, extra process methods such as z-tamping, steel rod post-tensioning, cylinder backpressure

control, MELT CORE printing head, compression wheel, and inbox printing platform were added and tested to lower these effects for better mechanical properties. These technologies mainly attempt to lower the void content of the printed structure, control the temperature development of the structure, control the melt flow of the extrudes, or post-tensioning the structure.

Z-tamping and compression wheel has a similar approach by filling the voids from the existing layer with a newly extruded layer. The vibration from the z-tamping and pressing from the compression wheel provides mechanical force to the newly extruded semi-molten melts onto the previous layer. During this process, formatted voids in previous layers get filled and higher adhesion between layers is brought.

The MELTCORE printing head by LSAM and in-box platform by THE BOX series has a strategy on controlling the temperature development of the process. The heat barrel, which is a part of the MELTCORE printhead, delivers uniform heat to the feedstock material-melts, bringing good control to the print bead. This influences in tighter print bead control and more accurate print structure. The printing process held in a box results in insulation and uniform ambient temperature to the printing extrudes and the structure. Compton et al. (2017) claimed the rise of the ambient temperature of the build chamber highly influences the success of large-scale produced parts. Therefore, it could be understood the temperature controls in THE BOX highly influences the structure to achieve good mechanical properties.

The backpressure applied on the cylinder of large-scale double-stage-screw direct pellet extruder and the MELTCORE printhead attempts on controlling the material melt flow. The increase of exerted pressure to the back of the cylinder increases the volumetric flow rate of the material-melts which leads to larger printing layer width. In small-scale FDM experiment, the increase of layer width resulted in higher void formation which led to lower mechanical properties. (Le Duigou et al. 2016.) However, in large-scale production, with an increase of layer width the layer height decreased which lead to enough bonding area. In addition, it could be assumed that better adhesion occurs due to larger beads having heavier weight. Also, with a larger width, the production speed could be accelerated as fewer nozzle passes are needed. The temperature development control of MELTCORE printing head eventually leads to control on the material melt flow bringing tighter control of print bead fusion. This results in a good fusion between layers with void-free structures.

The research project AMIE and Minibuilders have a similar approach to post-processing the structure. During the project AMIE, BAAM technology is used to produce a cylindrical-like architect structure. In

the BAAM technique, improvement of strength and modulus were shown by adjustment of process parameter however, research of Duty et al. (2017) claimed that high anisotropy value was shown at the produced parts which limit the application. Unlike the x and y-axis, the z-axis printing direction of BAAM in AMIE result in structural weakness, showing a high anisotropy value. Therefore, methods of reducing the degree of anisotropy were developed by post-tensioning the whole length of the structure with steel rods. In the last process of Minibuilders, the vacuum robot perpendicularly extruded reinforce layers to the structure built by the foundation robot and grip robot. Both methods mechanically added extra materials on the direction which could bring high failure points and reinforced the structure.

The C-FAB technology has a totally different production approach compared to the other large-scale gantry systems. Since C-FAB is a robotic system, it has a high flexible nozzle movement being able to have extrusion road beyond vertical and horizontal shapes. The extrusion roads of forming a structure were replicating a natural shape at a cellular level. In addition, the shape of the nozzle was design to extrude the melts in forms similarly to natural structures. These methods brought extremely strong tensile properties of end parts even though using low material amounts. Further, the nozzle cooling system was involved in the solidification process resulting in improvement on mechanical properties.

# 6 CONCLUSION AND OUTLOOK

In this thesis, a survey was conducted on recent developments and progress in FDM technique and large-scale direct pellet extrusion. The literature review covers reinforced polymer composite, parameters effecting the processing, and new approaches in processing methods to enhance the mechanical properties of the printed parts. Most of the research found in literature has been focused on reinforced polymer composites and adjusting the printing process to lower void formation and develop uniform property distribution in the end products. The presence of voids in structures decreased the bonding between layers. In addition, agglomerated fibers caused stress concentration resulting in lower mechanical properties of printed parts which led to the failure of the structure in the presence of load. Literature claimed that the fiber distribution of printed parts was mainly influenced by the composite filament production. Therefore, to gain uniform fiber distribution, a mixing process was added at the filament production.

Polymer composites reinforced with carbon, glass, wood, $TiO_2$, graphene, and microsphere resulted in an improvement on the tensile strength of end products. However, these polymer composites resulted in lower flexibility, limiting the range of product applications. The decreased flexibility was redeemed by addition of plasticizer, elastomer, or compatibilizer. An exception of reinforced polymer composite of Cu, Fe, TPE, and jute fiber showed opposite results by lower tensile strength and higher Young's modulus.

The tensile strength improved with an increase of reinforcing filler infill, however, after an optimum point, the effect started to decrease or show a plateau phenomenon due to inner-void formation, average fiber length decrease and fiber agglomeration which decreased the layer adhesion and produced stress concentration in printed parts. In one study, the decrease of layer adhesion by inner-void formation was adjusted with adding microsphere. (Wang et al., 2016.) The expansion of the microsphere during the heated printing, filled up the inner-void of the produced parts.

Additional printing parameters such as printing angle, printing width, printing layer height, and printing temperature effected the mechanical properties of the printed parts. Structures which contained a printing angle of 0°, the longitudinal direction, showed generally higher tensile properties with lower inner-void formation compared to other printing angles of 90°, 45°, -45°. The increase of printing width resulted in lack of melting and blending pressure, lower accuracy of the structure, higher void formation, and lower

layer adhesion however, acceleration on the printing process. Layer height showed different effects depending on the printing material. Generally, with lower layer height, mechanical properties increased however, in material such as graphene reinforced PLA resulted in an opposite effect. Often, the increase of printing temperature resulted in a higher volume flow rate of melts resulting in better adhesion between layers and tensile properties. A good mixture amount of polymer and fiber composite results in better mechanical properties at FDM printing process than CM, however, most of the literature claimed that CM brings better mechanical properties. Therefore, depending on the application characteristic, the process method of CM or FDM can be chosen.

Large-scale direct pellet extrusion can be mainly divided into two process method of the gantry and robotic system. Gantry system is very similar to FDM technology and the changes in process parameters show similar effects on the mechanical properties of printed products. The robotic system has high flexibility in process condition. Large-scale production has more radical influence with parameter changes resulting in higher void formation, shrinkage, and residual stress which leads to lower mechanical strength. Therefore, to redeem these effects extra process technologies were added such as z-tamping, steel rod post-tensioning, pressure adjusting, compression wheel, MELT CORE printing head, in-box platform, water cooling system, vacuum robot, and nozzle with flexible head.

Z-tamping in BAAM process produced vibration at the printer head to fill voids and improve layer adhesion. It resulted in significant improvement in tensile properties. Steel rod post-tensioning of AMIE research project improved lacking mechanical properties which were caused by z-axis printing direction. The increase of cylinder backpressure during the process of large-scale double-stage-screw direct pellet extruder increased the melt flow and improved the bonding of layers and mechanical properties. The MELT CORE printhead at LSAM leads better control of extruding beads with uniform heat distribution. Also, the compression wheel which forces the newly deposits onto the previous layer enhanced the fusion between the deposited layers resulting in better mechanical properties that can be used in industrial applications. THE BOX series showed successful printed parts by the factor printing process being held inside a box resulted in more uniform temperature development to the produced structure. Further, the cooling water system controlled the solidification of deposit layers leading to stronger structures. C-FAB technology which is a robotic system produces with a printing nozzle and deposition road which replicates the natural structure as the printing head has a flexible movement. This leads to lower material use and extremely strong tensile properties. Minibuilders have an extra robot that is attached to the produced structure through vacuum and moves up and down depositing melt layers

perpendicularly to the direction of the structure layers. This process reinforces the structure and leads to better mechanical properties.

In conclusion, the collected data from the literature gives a general view of the recent developments of FDM and large-scale direct pellet extrusion technology. Optimization of process parameters, reinforced composites, and the addition of extra process methods can lead to achieving improved mechanical properties. Therefore, depending on the application of technology, process adjustment can be made. FDM and large-scale direct pellet extrusion technology can be highly beneficial to the industry and the environment as it reduces material waste, energy consumptions, and production time compared to the traditional subtractive techniques. Nevertheless, considerably more research is to be done to reach comprehensive favored mechanical properties for industrial use.

**REFERENCES**

3d-printers. https://blbindustries.se. Accessed 22 July 2020.

About the 3d print canal house. https://3dprintcanalhouse.com. Accessed 23 July 2020.

Alani, T., F. Othman, and H. Ali. 2018. Investigation and analysis of infill density on impact property 5.

Baker, I. 2018. Polypropylene. Fifty Materials That Make the World, 169–173. Cham: Springer International Publishing.

Bashford, D. 1996. Thermoplastics. Dordrecht: Springer Netherlands.

Biswas, K., J. Rose, L. Eikevik, M. Guerguis, P. Enquist, B. Lee, L. Love, J. Green, and R. Jackson. 2017. Additive Manufacturing Integrated Energy—Enabling Innovative Solutions for Buildings of the Future. Journal of Solar Energy Engineering 139(1).

Boyd, R. P., C. Weller, A. Disanto, M. Rees, and B. Hilbert. 2017. Patent Application Publication. Cellular Fabrication and Apparatus for Additive Manufacturing. USA. US 20170217088.

Camargo, J. C., Á. R. Machado, E. C. Almeida, and E. F. M. S. Silva. 2019. Mechanical properties of PLA-graphene filament for FDM 3D printing. The International Journal of Advanced Manufacturing Technology 103(5–8) 2423–2443.

Campbell, F. C. 2010. Structural Composite Materials. ASM International.

Chacón, J. M., M. A. Caminero, E. García-Plaza, and P. J. Núñez. 2017. Additive manufacturing of PLA structures using fused deposition modelling: Effect of process parameters on mechanical properties and their optimal selection. Materials and Design 124, 143–157.

Compton, B. G., B. K. Post, C. E. Duty, L. Love, and V. Kunc. 2017. Thermal analysis of additive manufacturing of large-scale thermoplastic polymer composites. Additive Manufacturing 17, 77–86.

DeArmitt, C. 2017. Functional Fillers for Plastics. Applied Plastics Engineering Handbook, 517–532. Elsevier.

Delgado Camacho, D., P. Clayton, W. J. O'Brien, C. Seepersad, M. Juenger, R. Ferron, and S. Salamone. 2018. Applications of additive manufacturing in the construction industry – A forward-looking review. Automation in Construction 89, 110–119.

Dey, A., and N. Yodo. 2019. A Systematic Survey of FDM Process Parameter Optimization and Their Influence on Part Characteristics. Journal of Manufacturing and Materials Processing 3(3).

Din, S. H., M. A. Shah, N. A. Sheikh, and M. Mursaleen Butt. 2019. Nano-Composites and their Applications: A review. Characterization and Application of Nanomaterials 2(1), 1–9.

Dominghaus, H., J. Haim, and D. Hyatt. 1993. Plastics for engineers: materials, properties, applications. Hanser Publishers.

Duty, C. E., V. Kunc, B. Compton, B. Post, D. Erdman, R. Smith, R. Lind, P. Lloyd, and L. Love. 2017. Structure and mechanical behavior of Big Area Additive Manufacturing (BAAM) materials. Rapid Prototyping Journal 23(1), 181–189.

Fantuzzi, N., M. Bacciocchi, J. Agnelli, and D. Benedetti. 2020. Three-phase homogenization procedure for woven fabric composites reinforced by carbon nanotubes in thermal environment. Composite Structures 254.

Gebhardt, A., J.-S. Hötter. 2016. Basics, Definitions, and Application Levels. Additive Manufacturing, 1–19. Hanser.

German, R. M. 2016. Particulate Composites. Particulate Composites: Fundamentals and Applications. Cham: Springer International Publishing.

Gibson, I., D. Rosen, and B. Stucker. 2015. Additive Manufacturing Technologies. New York, NY: Springer New York.

Glass Transition Temperature (Tg) of Plastics - Definition & Values. https://omnexus.specialchem.com/polymer-properties/properties/glass-transition-temperature. Accessed 20 August 2020.

Grimm, T. 2002. Fused Deposition Modeling: A Technology Evaluation. T.A.Grimm & Associates, Inc.

Gupta, M. K., and J. Bijwe. 2020. A complex interdependence of dispersant in nano-suspensions with varying amount of graphite particles on its stability and tribological performance. Tribology International 142.

Hári, J., and B. Pukánszky. 2011. Nanocomposites. Applied Plastics Engineering Handbook, 109–142.

Heidari-Rarani, M., M. Rafiee-Afarani, and A. M. Zahedi. 2019. Mechanical characterization of FDM 3D printing of continuous carbon fiber reinforced PLA composites. Composites Part B: Engineering 175.

Heyman, S. 2017. Platt Boyd is branching out. Available : https://www.surfacemag.com/articles/architecture-architect-platt-boyd-3d-printing-branch-technology/. Accessed 23 August 2020.

Hodgson, G. Slic3r manual. Available: https://manual.slic3r.org/expert-mode/print-settings#fnref1.Accessed 20 August 2020.

Hull, C. 1986. 3d Systems Inc. Apparatus For Production Of Three-dimensional Objects By Stereolithography. USA: US 63890584 A.

Hwang, S., E. I. Reyes, K. Moon, R. C. Rumpf, and N. S. Kim. 2015. Thermo-mechanical Characterization of Metal/Polymer Composite Filaments and Printing Parameter Study for Fused Deposition Modeling in the 3D Printing Process. Journal of Electronic Materials 44(3), 771–777.

Iannace, S., L. Sorrentino, and E. Di Maio. 2014. Biodegradable biomedical foam scaffolds. Biomedical Foams for Tissue Engineering Applications, 163–187.

ISO/ASTM 52900-15. Standard terminology for additive manufacturing -general principles-terminology. 2015. ASTM international

Jakupovic, A. 2016. Mini Builders Project. 3D Printhuset A/S.

Jeffrey, C. 2014. Team of 3D-printing "minibuilder" robots print large-scale structures on site. Available: https://newatlas.com/minibuilder-robots-3d-print-large-scale-structures/32573/. Accessed 24 August 2020.

Jiang, L., and J. Zhang. 2017. Biodegradable and Biobased Polymers. Applied Plastics Engineering Handbook: Processing, Materials, and Applications, Second Edition.

Ke, J., Z. Wu, Y. Liu, Z. Xiang, and X. Hu. 2020. Design method, performance investigation and manufacturing process of composite helical springs: A review. Composite Structures 252.

Keshavamurthy, R., V. Tambrallimath, and D. Saravanabavan. 2021. Development of Polymer Composites by Additive Manufacturing Process. Reference Module in Materials Science and Materials Engineering.

Kraxner, M. 2002. Mechanical Process Engineering. Management center innsbruck, Innsbruck.

Krishnaprasad, R., N. R. Veena, H. J. Maria, R. Rajan, M. Skrifvars, and K. Joseph. 2009. Mechanical and Thermal Properties of Bamboo Microfibril Reinforced Polyhydroxybutyrate Biocomposites. Journal of Polymers and the Environment 17(2), 109–114.

Le Duigou, A., M. Castro, R. Bevan, and N. Martin. 2016. 3D printing of wood fibre biocomposites: From mechanical to actuation functionality. Materials & Design 96, 106–114.

Li, H., T. Wang, J. Sun, and Z. Yu. 2018. The effect of process parameters in fused deposition modelling on bonding degree and mechanical properties. Rapid Prototyping Journal.

Li, N., Y. Li, and S. Liu. 2016. Rapid prototyping of continuous carbon fiber reinforced polylactic acid composites by 3D printing. Journal of Materials Processing Technology 238, 218–225.

Liu, X., B. Chi, Z. Jiao, J. Tan, F. Liu, and W. Yang. 2017. A large-scale double-stage-screw 3D printer for fused deposition of plastic pellets. Journal of Applied Polymer Science 134 (31).

Love, L. J., V. Kunc, O. Rios, C. E. Duty, A. M. Elliott, B. K. Post, R. J. Smith, and C. A. Blue. 2014. The importance of carbon fiber to polymer additive manufacturing. Journal of Materials Research, 1893-1898.

Marrett, D. 2018. The Secret to LSAM Print Quality…A Different Process. Available: http://blog.thermwood.com/the-secret-to-lsam-print-quality-a-different-process. Accessed 22 July 2020.

Matsuzaki, R., M. Ueda, M. Namiki, T.-K. Jeong, H. Asahara, K. Horiguchi, T. Nakamura, A. Todoroki, and Y. Hirano. 2016. Three-dimensional printing of continuous-fiber composites by in-nozzle impregnation. Scientific Reports 6(1).

Minibuilders -small robots printing large-scale structures. Available: https://iaac.net/project/minibuilders/. Accessed 24 August 2020.

Molitch-Hou, M. 2018. Overview of additive manufacturing process. Additive Manufacturing, Butterworth-Heinemann, 1–38.

Munz, O. 1956. Photo-glyph Recording. USA. US 2775758 A

Onwubolu, G. C., and F. Rayegani. 2014. Characterization and Optimization of Mechanical Properties of ABS Parts Manufactured by the Fused Deposition Modelling Process. International Journal of Manufacturing Engineering (2014), 1-13.

Paolini, A., S. Kollmannsberger, and E. Rank. 2019. Additive manufacturing in construction: A review on processes, applications, and digital planning methods. Additive Manufacturing 30 (July), 100894.

Park, S.-J., and M.-K. Seo. 2011. Element and Processing. 431–499.

Peltola, H. 2019. Morphological effects of lignocellulosic fibers on poly (lactic acid) biocomposites. Tampere university. Faculty of engineering and natural sciences. PhD Thesis.

PLA vs ABS Filament - Plastic strength, flexibility compared! Buyer's guide 2020. Article on the website of Allthat3D. https://www.allthat3d.com/pla-vs-abs/. Accessed 20 August 2020.

Pollack, S., C. Venkatesh, M. Neff, A. V. Healy, G. Hu, E. A. Fuenmayor, J. G. Lyons, I. Major, and D. M. Devine. 2019. Polymer-Based Additive Manufacturing: Historical Developments, Process Types and Material Considerations. Polymer-Based Additive Manufacturing. Cham: Springer International Publishing. 1–22.

Process. Article on the website of branch technology. https://www.branch.technology/process. Accessed 23 August 2020.

Rethwisch, D. G., and W. D. Callister. 2015. Fundamentals Materials science and Engineering : An Integrated Approach. Fundamentals of Materials Science and Engineering AN INTEGRATED APPROACH (5th Edition),1–964.

Sezer, H. K., and O. Eren. 2019. FDM 3D printing of MWCNT re-inforced ABS nano-composite parts with enhanced mechanical and electrical properties. Journal of Manufacturing Processes 37 (2019), 339–347.

Sharma, R., R. Singh, R. Penna, and F. Fraternali. 2018. Investigations for mechanical properties of Hap, PVC and PP based 3D porous structures obtained through biocompatible FDM filaments. Composites Part B: Engineering 132 (2018), 237–243.

Shofner, M. L., K. Lozano, F. J. Rodríguez-Macías, and E. V. Barrera. 2003. Nanofiber-reinforced polymers prepared by fused deposition modeling. Journal of Applied Polymer Science 89 (11), 3081–3090.

Sin, L. T., R. R. Rahmat, and W. A. W. A. Rahman. 2012. Polylactic Acid: PLA Biopolymer Technology and Applications. Polylactic Acid: PLA Biopolymer Technology and Applications. Elsevier Inc.

Sodeifian, G., S. Ghaseminejad, and A. A. Yousefi. 2019. Preparation of polypropylene/short glass fiber composite as Fused Deposition Modeling (FDM) filament. Results in Physics 12 (2019), 205–222.

Spruck, M. 2019. Plant & process engineering. Management center innsbruck, Innsbruck

Stress-strain diagrams (LearnChemE). 2011. Video on Youtube. Accessed: https://www.youtube.com/watch?v=t9eB0PKYAt8. Accessed on 20 August 2020.

Sukindar, N. A., M. K. A. Ariffin, B. T. H. T. Baharudin, C. N. A. Jaafar, and M. I. S. Ismail. 2016. Analyzing the effect of nozzle diameter in fused deposition modeling for extrusing polylactic acid using open source 3D printing. Jurnal Teknologi 78 (10).

Tekinalp, H. L., V. Kunc, G. M. Velez-Garcia, C. E. Duty, L. J. Love, A. K. Naskar, C. A. Blue, and S. Ozcan. 2014. Highly oriented carbon fiber–polymer composites via additive manufacturing. Composites Science and Technology 105, 144–150.

Torrado Perez, A. R., D. A. Roberson, and R. B. Wicker. 2014. Fracture Surface Analysis of 3D-Printed Tensile Specimens of Novel ABS-Based Materials. Journal of Failure Analysis and Prevention 14 (3), 343–353.

Tronvoll, S. A., T. Welo, and C. W. Elverum. 2018. The effects of voids on structural properties of fused deposition modelled parts: a probabilistic approach. The International Journal of Advanced Manufacturing Technology 97 (9–12), 3607–3618.

Tymrak, B. M., M. Kreiger, and J. M. Pearce. 2014. Mechanical properties of components fabricated with open-source 3-D printers under realistic environmental conditions. Materials and Design 58 (2014), 242–246.

Wainwright, O. 2014, March 28. Work begins on the world's first 3D-printed house. The Guardian. Amsterdam.

Walsh, T. 2017. The Plastic Piping Industry in North America. *In* Applied Plastics Engineering Handbook, 697–716. Elsevier.

Wang, J., H. Xie, Z. Weng, T. Senthil, and L. Wu. 2016. A novel approach to improve mechanical properties of parts fabricated by fused deposition modeling. Materials & Design 105, 152–159.

Wang, X., M. Jiang, Z. Zhou, J. Gou, and D. Hui. 2017. 3D printing of polymer matrix composites: A review and prospective. Composites Part B: Engineering 110, 442–458.

Wu, P., J. Wang, and X. Wang. 2016. A critical review of the use of 3-D printing in the construction industry. Automation in Construction 68, 21–31.

Wu, W., P. Geng, G. Li, D. Zhao, H. Zhang, and J. Zhao. 2015. Influence of Layer Thickness and Raster Angle on the Mechanical Properties of 3D-Printed PEEK and a Comparative Mechanical Study between PEEK and ABS. Materials 8(9), 5834–5846.

Zhong, W., F. Li, Z. Zhang, L. Song, and Z. Li. 2001. Short fiber reinforced composites for fused deposition modeling. Materials Science and Engineering: A 301(2), 125–130